



Contents lists available at ScienceDirect

Arabian Journal of Chemistry

journal homepage: www.ksu.edu.sa

Original article

Nanocomposite ZIF-8@Active Carbon-co-Chitosan incorporated nanofiltration membrane with enhanced antifouling property and high separation efficiency to salt, heavy metals, and dye solutions

Mina Afshari, Abdolreza Moghadassi*, Sayed Mohsen Hosseini*

Department of Chemical Engineering, Faculty of Engineering, Arak University, Arak 38156-8-8349, Iran



ARTICLE INFO

Keywords:

Nanofiltration
ZIF-8@(AC-co-CS) nanocomposite
Dye/Salt/Heavy Metal removal
High flux/rejection
Antifouling ability

ABSTRACT

Nanocomposite Zeolitic imidazolate framework (ZIF-8)@ Active Carbon (AC)-co-Chitosan (CS) was employed to fabricate polyether sulfone-based nanofiltration membranes. The ZIF-8@(AC-co-CS) nanocomposite was synthesized using a simple co-precipitation method and examined by field emission scanning electron microscope (FESEM) images, Attenuated total reflectance-Fourier transform infrared (ATR-FTIR) analysis, and X-ray diffraction pattern (XRD). Membrane properties used analyses such as FESEM, ATR-FTR, atomic force microscopy (AFM), porosity, water content, contact angle measurements, roughness assessment, pure water flux (PWF), separation efficiency evaluation, and fouling analysis. The surface roughness of the membrane with 0.01 wt% ZIF-8@(AC-co-CS) was nearly half that of the pristine membrane. Investigation outcomes revealed more excellent hydrophilicity for modified membranes. The water flux measured over three times greater for modified membranes than pristine ones. All modified membranes exhibited noteworthy rejection of sodium sulfate, achieving levels exceeding >93 %. The nanocomposite membrane was also assessed for removing two heavy metal ions, i.e., Cu and Cr. The results indicated a 55.0 % removal for Cu and 62.3 % removal for Cr by the virgin membrane, while that was >94 % and >97 % for the modified membrane, respectively. Also, higher separation efficiency was achieved for chromium ions compared to copper ions by the membranes. The nanocomposite membranes exhibited impressive dye rejection rates: >97 % for Methylene Blue, >95 % for Rhodamine B, >92 % for RB50, >94 % for RB21, >89 % for RY145, and >86 % for RY39. The FRR parameter significantly increased to >97 % for the modified samples. The nanofiltration performance of ZIF-8@AC-co-CS nanocomposite membranes exhibited a remarkable improvement compared to CS-based membranes.

1. Introduction

Ensuring superior water quality is crucial in addressing the diverse requirements of businesses and communities. Water treatment is necessary to offset shortages (Langbehn et al., 2021, Varma et al., 2024). In this case, rising urbanization and industrialization, which hasten industrial emissions of dangerous organic and inorganic pollutants, have drawn attention to the need for environmentally friendly wastewater treatment and reuse to supply high-quality, sustainable water (Amiri et al., 2021, Edo et al., 2024). One of the most problematic types of polluted wastewater is colored wastewater, which is problematic due to its hazardous compounds and the high volume of dyes used in various industries (Hema and Arivoli 2007, Liu and Wang 2024). Dyes, the most detected pollutant in wastewater, comprises several compounds, such as

metals, aromatic rings, and other hazardous materials. Moreover, dyes may harm humans, contributing to disorders of the central nervous system, liver, and kidneys (Giri and Badwaik 2022). Scientists have employed various methods to solve this issue, including using nanoparticles and membranes. Recently, the release of heavy metals into the environment has become another issue associated with industry and modernization. This pollution is detrimental to humans and may result in various illnesses, including cancer and genetic problems. One of the challenges in water purification is the removal of heavy metals at low concentrations, a task achievable through membrane-based systems. In this context, researchers are investigating advanced techniques to improve membrane filtration efficiency (Shukla et al., 2021). Membrane filtration removes pollution from industrial wastewater. The filtration membrane does not require high energy or phase change, so it is more

* Corresponding authors.

E-mail addresses: a-moghadassi@araku.ac.ir (A. Moghadassi), s-hosseini@araku.ac.ir (S. Mohsen Hosseini).<https://doi.org/10.1016/j.arabjc.2024.105951>

Received 28 February 2024; Accepted 5 August 2024

Available online 6 August 2024

1878-5352/© 2024 The Authors. Published by Elsevier B.V. on behalf of King Saud University. This is an open access article under the CC BY-NC-ND license (<http://creativecommons.org/licenses/by-nc-nd/4.0/>).

effective than alternative methods. Reverse osmosis (RO) and nanofiltration (NF) are the separating membranes that are most often employed, but lowering operating pressure with appropriate efficiency is NF's benefit over RO (Miao et al., 2008, Hosseini et al., 2019, Morgante et al., 2024). Nanofiltration commonly utilizes polymeric membranes due to their advantages, such as ease of production, adaptability, and the ability to select from various materials. However, the drawback of using polymeric membranes is fouling, which can reduce the efficiency and lifespan of the membrane. A research study on polyvinylidene fluoride (PVDF)-based membrane found a 43 % reduction in flux due to fouling (Kharraz and An 2020). Fouling not only reduces the efficiency of the membrane but also increases energy consumption. As the fouling layer accumulates, the pressure drop across the membrane increases, requiring higher energy input to keep the desired flow rate. A study on a polymeric membrane found that a 35 % increase in transmembrane pressure was needed to maintain the initial flux due to fouling (Ullah et al., 2021). A significant challenge for polymeric membranes is enhancing their anti-fouling properties, which depend on the surface roughness and hydrophilicity of the membrane. Membranes with higher hydrophilic properties can absorb more water molecules on their surface, which helps to remove undesirable particles from the surface through water flows. Research indicates that membranes with smoother surfaces and less roughness exhibit better antifouling properties. Rough surfaces trap various particles, which negatively impacts the membrane's performance (Li et al., 2023, Wang et al., 2023).

Polyethersulfone (PES) is an industrial-grade polymer known for its advantageous physical and chemical characteristics, making it a well-suited material for fabricating membranes used in wastewater treatment. Its processability, heat resistance, and capacity to endure diverse environmental conditions collectively make it an apt choice. One of the critical advantages of PES is its excellent thermal stability. It can tolerate elevated temperatures without experiencing substantial degradation or performance loss. This property is crucial in membrane-based separation that involves elevated temperatures, such as water treatment systems or industrial processes (Alenazi et al., 2017). Another essential advantage of PES-included membranes is their outstanding chemical resistance. They resist various chemicals, including acids, bases, and organic solvents. This makes PES membranes suitable for applications where exposure to aggressive chemical environments is expected, such as desalination (Choi et al., 2018, Eskikaya et al., 2024, Oulad et al., 2024). To better manage the membrane's hydrophobic and hydrophilic properties, the structure of the nanofiltration membrane has been modified. One membrane method is bulk modification, in which structural alterations are made to the polymer in bulk before the membrane is produced to improve its general qualities. Incorporating nanomaterials to modify membranes is among the most feasible techniques (Farahani and Hosseini 2022, Hosseini et al., 2023). The advantages of combining nanomaterials to modify membranes are numerous and promising. These modifications enhance selectivity, Permeability, mechanical strength, stability, and multi-functionality (Goh et al., 2016, Fan et al., 2023). Researchers commonly enhance blended membranes with various nanomaterials, including mineral metal nanomaterials, chitosan-based nanoparticles, and porous substances like metal-organic frameworks (MOFs). These nanomaterials are integrated into the membranes to improve their hydrophobic properties, enhance resistance to fouling, and increase separation capabilities (Sinha Ray et al., 2020, George and Kumar 2023). MOFs are famous for creating blended membranes because of their hydrophilic specific surface, which improves the performance of polymer-based membranes like (PVDF) or PES (Sharma et al., 2023, Zhao et al., 2023, Zheng et al., 2023). In conclusion, MOFs are nanoporous materials of metal ions and organic ligands, forming a crystalline structure. These materials are known for their large surface area, porous structure, and ability to be modified, rendering them highly versatile across various applications such as drug delivery, gas separation, and catalysis, as well as adsorptive removal, separation, and purification. Moreover, MOFs possess qualities that enhance the

hydrophilicity of membranes (Furukawa et al., 2013, Goh and Ismail 2018, He et al., 2024, Shahid et al., 2024, Shao et al., 2024).

Due to its adsorptive solid properties, chitosan can effectively adsorb various metal ions and organic dyes through its numerous amine and hydroxyl groups. Chitosan is a biodegradable substance that is non-toxic and hydrophilic. Chitosan's unique qualities facilitate the production of adsorbents and their use in membrane applications (Batool et al., 2023). Bagheripour et al. incorporated graphene oxide (GO) /chitosan (CS) nanocomposite to modify the surface of a polyethersulfone NF membrane, enhancing its ability to separate various metals. They found that adding 1 % composite nanoparticles to the membrane resulted in a uniform distribution of nanoparticles, reducing surface roughness and improving anti-fouling properties (Bagheripour et al., 2018). Due to their exceptional potential, carbon-based nanomaterials have also received a lot of interest in manufacturing and modifying membranes. Active carbon nanoparticles (ACNP) are appropriate for membrane applications due to their high aspect ratios, specific surface areas, excellent mechanical properties, partial negative charge, and adsorption behavior. According to past investigations, adding ACNP to polymeric membranes improved their suitability for physicochemical applications. According to past investigations, adding ACNP to polymeric membranes improved their physicochemical application characteristics, mechanical stability, and separation performance (Hosseini et al., 2018, Abid et al., 2022, Natrayan et al., 2022, Khan and Ahmad 2023, Sharma et al., 2023, Wu et al., 2023). Hosseini and his team developed a PES membrane with a nanoparticle (Carbon Nanofibers/CS) for surface modification and metal removal. The modified membrane showed 16 % more sodium salt sulfate rejection than the unmodified membrane. The nanoparticle-based membrane also allowed more than three times more flux passage than the bare membrane. The removal of heavy metals copper, chromium, and lead was significantly higher than the pristine membrane (Hosseini et al., 2021). Due to the material's benefits, researchers are paying increasing attention to using MOF materials in fabricating NF membranes to create composite membranes. In addition, by modifying the structure of MOFs with a guest matrix, it is possible to improve pore selectivity and make an arrangement with high compassion in the mixed matrix membrane (MMM). Khajavian et al. prepared a CS/Polyvinyl alcohol/ Zeolitic imidazolate framework (ZIF-8) thin film composite adsorptive membrane with PVDF membrane support, resulting in an up to 8 % increase in flux and rejection (Khajavian et al., 2020). In another study, Moutloali and his colleagues fabricated ultrafiltration (UF) membranes from the combination of Ag@ZIF-8@GO, Cu@ZIF-8@GO, Ag-Cu@ZIF-8@GO, and Cu(tpa)@GO with polyethersulfone. The MOF/PES membranes have the potential for water purification and recovering heavy metals, such as silver. (Makhetha and Moutloali 2018, Makhetha and Moutloali 2021). Kamari and his colleagues conducted a study to investigate the effects of incorporating Fe₃O₄@SiO₂-CS bio-nanocomposite as an additive in PES nanocomposite nanofiltration membranes. The modified membrane effectively removes heavy metals at 98.11 %, 98.61 %, and 98.86 % for Pb²⁺, Cu²⁺, and Cr²⁺. It also offers favorable pure water flux and effective resistance to fouling (Kamari and Shahbazi 2021). Mengjie et al. embedded the UiO-66-NH₂/ZIF-8 nanocomposite into the NF membrane to enhance its dye rejection, Permeability, and anti-fouling efficiency. The outcome illustrated good antifouling capability and high dye rejection for the UiO-66-NH₂/ZIF-8/PES membranes (Fu et al., 2022).

ZIF-8, a variant of MOFs categorized within the family of zeolitic imidazolate frameworks, possesses several merits, including an expansive specific surface area, a consistent arrangement of pores, chemical stability, easy customization, and a straightforward synthesis process (Wang et al., 2019, Shao et al., 2024). Combining ZIF-8, AC, and CS creates nanocomposites that effectively adsorb pollutants with high performance (Bao et al., 2013, Keshvardostchokami et al., 2021, Al-Hazmi et al., 2022).

Since most research has focused on evaluating MOF modifications in solution-based environments, we expect that integrating the developed

nanocomposite into PES-based nanofiltration membranes will effectively address various pollutants, inclusive of dyes, heavy metals, and the facilitation of desalination. Also, previous research on removing contaminants by ZIF-8, AC, and CS led us to merge and modify the shape of these materials for amendment and to address PES membrane flaws. Currently, limited research is available on the impact of ZIF-8@(AC-co-CS) nanocomposite in the context of membrane separation applied to water filtration. Additionally, there is insufficient existing literature concerning the creation and analysis of nanofiltration membranes based on mixed matrix PES, which has been altered using the ZIF-8@(AC-co-CS) nanocomposite. Therefore, this study aimed to create the MMM nanofiltration membranes by incorporating the synthesized ZIF-8@(AC-co-CS) nanocomposite and to investigate the influence of different loading ratios of the additive into the membrane structure on their physicochemical properties, separation performance, and antifouling capabilities. In this study, various solutions, such as Methylene Blue (MB), Rhodamine B (RhB), four reactive dyes, heavy metals, Na_2SO_4 , and MgSO_4 , were used to evaluate the effectiveness of the prepared membranes in terms of their separation performance.

2. Experimental

2.1. Material

Zinc nitrate hexahydrate ($\text{Zn}(\text{NO}_3)_2 \cdot 6\text{H}_2\text{O}$, 99 % purity), 2-methylimidazole (Hmim, 99 % purity), and dimethylacetamide (DMAc, purity > 99 %) were acquired from Merck Co., Germany. Merck Co., Germany, supplied Na_2SO_4 , MgSO_4 , CrSO_4 , and CuSO_4 . Merck Inc.,

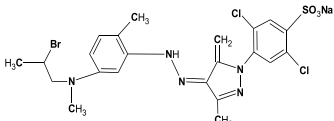
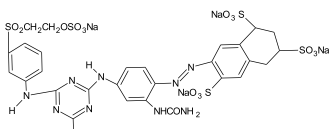
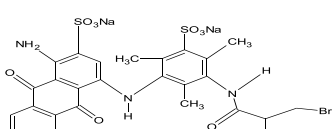
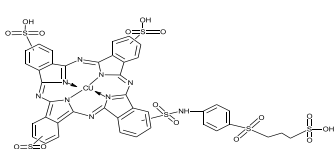
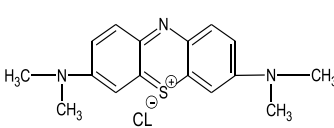
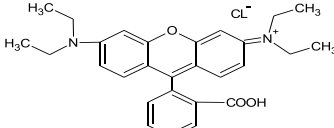
Germany, Polyvinylpyrrolidone (PVP, $M_w = 25$) was sourced from Merck Inc., Germany. Across Inc., USA supplied chitosan (CS, $M_w = 100,000\text{--}300,000$, 90 % deacetylated). Activated carbon nanoparticles (ACNP, black powder, spherical, specific surface area (SSA) > $1000 \text{ m}^2/\text{g}$, 0.43 g/l) were obtained from US Research Nanomaterial, Inc., USA. We used distilled water exclusively during the experiment.

Reactive yellow 39 (RY39), reactive yellow 145 (RY145), reactive blue 50 (RB50), reactive blue 21 (RB21), rhodamine B (RhB), and methylene blue (MB) were obtained from Saujanya in Mumbai, India. Table 1 presents the molecular structure, pH, charge, and maximum absorption wavelength (nm) of each dye.

2.2. Synthesis of activated carbon-co-chitosan composite nanoparticles

Previous literature provides a detailed description of the process for synthesizing AC-co-CS nanoparticles (Ebrahimi et al., 2019). First, we prepared two solutions: one with CS in 2 wt% hydrochloric acid at a concentration of 1 wt%, which was filtered to eliminate impurities, and the other with 5 wt% in ethanol, relative to the weight of CS. We vigorously mixed both solutions at ambient temperature. Subsequently, the ACNP solution was fused with the CS solution and actively mixed for four hours, with ultrasonic treatment for 30 min, to ensure uniformity of the nanocomposite. The AC-co-CS composite particles were then precipitated with a mixture of ethanol and sodium hydroxide, followed by rinsing with distilled water until neutralizing. We dried the composite at 60°C for 12 h.

Table 1
The characteristics of the dyes employed in this investigation.

Color	pH	Charge	Maximum Absorption Wavelength (nm)	Structure
Reactive Yellow 39	7.00	Anionic	419	
Reactive Yellow 145	6.97	Anionic	418	
Reactive Blue50	6.39	Anionic	595	
Reactive Blue 21	7.00	Anionic	626	
Methylene Blue	7.00	Cationic	664	
Rhodamine B	7.00	Cationic	554	

2.3. Synthesis of ZIF-8@(AC-co-CS) nanocomposite

We produced the ZIF-8@(AC-co-CS) using a simple co-precipitation method (Cao et al., 2017, Khajavian et al., 2020). $\text{Zn}(\text{NO}_3)_2 \cdot 6\text{H}_2\text{O}$ (2.93 g) was dissolved separately with 10 mg of AC-co-CS composite nanoparticles, while Hmim (6.48 g) was dissolved in 12.11 g and 48.45 g of distilled water, respectively. The ratio of ZIF-8 to AC-co-CS in this study is approximately 0.05. Next, we mixed and agitated both sample solutions at 30 °C for 30 min. The resulting white precipitate, identified as ZIF-8@(AC-co-CS), was then separated from the mixture via centrifugation. Afterward, the ZIF-8@(AC-co-CS) precipitate was thoroughly cleaned with ethanol and gently rinsed with distilled water. Finally, we dried the material at 60 °C for 12 h.

2.4. Fabrication of the MMM

The phase inversion technique creates polymeric nanofiltration membranes. We added different concentrations of ZIF-8@(AC-co-CS) nanocomposite at three levels—high (1 wt%), medium (0.01 and 0.1 wt%), and low (0.001 and 0.005 wt%) to DMAc solvent. The mixture was then exposed to ultrasonic treatment for 20 min to achieve uniform dispersion of the nanocomposites. Next, we incorporated 1 wt% PVP and 18 wt% PES into the mixture to create a homogeneous solution, which we stirred for 24 h. The solution was allowed to rest for a day to eliminate any trapped air bubbles. Subsequently, the solution was applied onto a clean glass substrate using a casting knife with a thickness of 170 μm . The MMM was swiftly fully submerged in a non-solvent bath of distilled water. Finally, we immersed the MMM in deionized water for an additional day to ensure that all remaining solvents were thoroughly removed (Moghadassi et al., 2023). Table 2 provides the details of the polymeric solutions used in the combination.

2.5. Analytical methods

To characterize the synthesized AC-co-CS and ZIF-8@(AC-co-CS) nanocomposites, we used several techniques, including X-ray diffraction pattern (XRD, Philips PW 1730 diffract meter), field emission scanning electron microscope (FESEM, Tescan-Mira III, Check Republic), dynamic light scattering (DLS, Malvern, Zeta sizes pro and ultra, United Kingdom), and Attenuated total reflectance-Fourier transform infrared (ATR-FTIR, ABB Bomem-MB-104, Switzerland). Furthermore, we used mapping analysis procedures to generate images of the nanoparticles and to illustrate their distribution within the membrane structure. We examined the membrane morphology and pore shape by capturing surface and transverse cross-section images using FESEM and atomic force microscopy (AFM, Dimension Icon, Bruker, Germany). To prepare the membrane for FESEM analysis, we first froze the sample in liquid nitrogen, then broke it into pieces. Additionally, from the surface of the membranes, we captured the AFM images with an $8 \times 8 \mu\text{m}$ scanning area. We also used the DME-SPM software (version 2.1.1.2) to calculate the roughness parameters. Additionally, we determined the overall porosity of both unmodified and modified membranes by employing the gravimetric method, as described by Equation (1) (Hosseini et al., 2019). The pH was measured using a pH meter (Jenway 3510 Standard Digital pH Meter Kit; 230 VAC/UK).

Table 2
The formulation of the casting solution for the membrane samples.

Sample	PES (wt%)	PVP (wt%)	DMAc (wt%)	ZIF-8@(AC-co-CS) (wt%)
M ₀	18	1	81.000	0.000
M ₁	18	1	81.999	0.001
M ₂	18	1	81.995	0.005
M ₃	18	1	81.990	0.010
M ₄	18	1	81.900	0.100
M ₅	18	1	80.000	1.000

We used Equation (1) to calculate the total porosity of the membranes.

$$\varepsilon (\%) = \left(\frac{W_w - W_d}{A \times d_w \times L} \right) \times 100 \quad (1)$$

W_w and W_d represent the weight of the membranes after drying and when wet, respectively. In this context, A represents surface area, d_w represents water density, and L stands for the thickness of the membrane.

We used the Guerout-Elford-Ferry equation (Equation (2)), which takes into account the operating pressure (ΔP) at 0.4 MPa, permeated water (Q) in m^3/s , and water viscosity (η), which is 8.9×10^{-4} Pa.s.

$$rm = \sqrt{\frac{(2.9 - 1.75\varepsilon) \times 8\eta LQ}{\varepsilon A \Delta P}} \quad (2)$$

2.6. Permeability, fouling resistance, and separation efficiency of the MMM

We evaluated the performance of the fabricated membranes by measuring pure water flux (PWF), permeability of powdered milk solution, and removal of various substances, including Na_2SO_4 and MgSO_4 salt solutions, six different dyes, and heavy metal solutions. The dead-end modules utilized a functional area of 19.6 cm^2 to conduct the experiments. Initially, the MMM was exposed to distilled water at a pressure of 5 bar for 30 min to compact the MMM structure. Subsequently, we lowered the pressure to 4.5 bar to achieve a more consistent flow during the separation process. To reduce solute accumulation near the membrane, we stirred the feed solutions at 500 revolutions per minute (rpm) throughout the experimental process. The pure water flux was calculated by Eq. (3) (Hosseini et al., 2023).

$$J = \frac{V}{A \Delta t} \quad (3)$$

In this equation, J represents the net water flux ($\text{lit}/\text{m}^2 \cdot \text{hr}$), V (lit) is the collected water volume (lit), A is the surface area of the membrane (m^2), and Δt is the filtration process time (h).

The densities of the solutions employed to assess the separation capability of the membranes were as follows: a saline solution at 1000 ppm, heavy metal solutions at 20 ppm, a dye solution at 100 ppm, and a milk powder solution at 250 ppm. Following the filtration process, the efficiency of the membranes in removing these substances was evaluated using Eq. (4) (Daneshvar et al., 2005). The initial and final concentration of dye in feed and permeate sides were determined using a UV-2450 model UV-VIS spectrophotometer (Shimadzu, Japan) at different λ_{max} of different dyes (Table 1), and the dyes rejection was calculated by (Moradi et al., 2021):

$$R\% = \left(\frac{C_f - C_p}{C_f} \right) \times 100 \quad (4)$$

The value of C_p (mol/L) represents the pollutant amount present in the feed, while C_f (mol/L) is the level of pollutants in the permeated stream. In other words, C_p refers to the number of contaminants in the filtered material, while C_f indicates the degree of contaminant removal achieved by the filtration process.

To evaluate the anti-fouling properties of the produced membranes, we conducted a three-step test and employed Equation (6) to calculate the flux recovery ratio (FRR). In the first step, pure water was allowed to pass through the membranes at 0.45 MPa for an hour, and we measured the permeate flux (J_{w1} , $\text{L}/\text{m}^2 \cdot \text{h}$). During the second step of the process, we filtered a 250 ppm powdered milk solution and recorded the permeation flux (J_p , $\text{L}/\text{m}^2 \cdot \text{h}$). In the final stage, the fouled membranes were rinsed with distilled water for 20 min, and we measured the permeate flux again to determine its value for an hour (J_{w2} , $\text{L}/\text{m}^2 \cdot \text{h}$) (Childress and Elimelech 2000). It is important to note that various

equations exist to investigate membrane fouling, and the FRR calculation provides insight into the resistance of the membrane against fouling and its ability to maintain the permeate flux (Karan et al., 2015, Rezanian et al., 2019).

$$FRR\% = \left(\frac{J_{w,2}}{J_{w,1}} \right) \times 100 \quad (5)$$

Fouling parameters encompassing irreversible fouling (R_{ir}), reversible fouling (R_r), and overall fouling (R_t) were quantified utilizing Eqs.6–8 (Low et al., 2018, Farjami et al., 2021).

$$R_{ir}\% = (1 - FRR) \times 100 \quad (6)$$

$$R_r\% = \left(\frac{J_{w,2} - J_p}{J_{w,1}} \right) \times 100 \quad (7)$$

$$R_t\% = 1 - \left(\frac{J_p}{J_{w,1}} \right) \times 100 \quad (8)$$

Irreversible fouling occurs when washing fails to remove contaminant particles trapped within the pores of the membrane.

For more information, we also calculated the intrinsic resistance of the membrane (R_m), the cake resistance (R_c), the pore resistance (R_p), and the total filtration resistance (R_t) for our analysis. These values will provide a more detailed understanding of the filtration process (Farjami et al., 2019).

3. Results and discussion

3.1. Characterization of AC-co-CS and ZIF-8@(AC-co-CS) nanocomposites

To distinguish between AC-co-CS nanoparticles and ZIF-8@(AC-co-CS) nanocomposites, various analyses were conducted, including ATR-FTIR, XRD, FESEM, mapping analysis procedure images (MAP images), EDAX, and DLS have been carried out. Fig. 1 shows the results obtained from ATR-FTIR and XRD analyses. In Fig. 1(a), the signal

identified at 3181 cm^{-1} within AC-co-CS indicates the existence of functional groups such as O–H and –NH. Furthermore, the signals noted at 3000 and 2923 cm^{-1} substantiate the presence of C–H functional groups. ATR-FTIR spectra have highlighted diverse functional groups within the AC-co-CS structure, encompassing C = O and –NH₂ groups at 1570 cm^{-1} and 1422 cm^{-1} . Additionally, the peaks observed at 1178 cm^{-1} , 1146 cm^{-1} , 1103 cm^{-1} , and 958 cm^{-1} suggested the presence of C–O–C bonds, as well as the peaks observed at 684 cm^{-1} , 621 cm^{-1} indicate the hydroxyl, amine, and carboxyl functional groups (Ebrahimi et al., 2019). These wavenumbers correspond to out-of-plane bending vibrations and complex vibrational modes characteristic of these functional groups. We attribute the presence of these groups to the interactions and structure of the AC-co-CS polymer, which incorporates multiple functional groups, each contributing to the overall vibrational spectrum. The peak at 684 cm^{-1} is typically associated with bending vibrations of hydroxyl groups (–OH) and, in certain contexts, may also reflect the presence of carboxyl groups (–COOH). Conversely, the peak at 621 cm^{-1} is primarily attributed to the bending vibrations of amine groups (–NH₂) and can sometimes overlap with the bending vibrations of carboxyl groups. This overlapping of absorption bands explains the apparent presence of multiple functional groups at these wavenumbers (Farahani and Hosseini 2022). These findings were consistent with previous studies and supported the proper characterization of AC-co-CS. Hosseini et al. verified the ATR spectral bands corresponding to AC-co-CS (Ebrahimi et al., 2019). Fig. 1(a) also displays the ATR-FTIR spectrum of the ZIF-8@(AC-co-CS) nanocomposite. The ATR-FTIR spectrum of ZIF-8@(AC-co-CS) nanocomposites shows vibrational bands in the ranges of 621 – 1308 and 1308 – 1500 cm^{-1} , which were linked to the bending and stretching vibrations of the imidazole ring. Furthermore, a distinct peak at 423.15 cm^{-1} was attributed to the Zn stretching vibration, confirming the successful synthesis of the ZIF-8@(AC-co-CS) nanocomposite and the presence of known functional groups (Xiong et al., 2022).

Fig. 1(b), (c) illustrates the XRD patterns of AC-co-CS and ZIF-8@(AC-co-CS) nanocomposites. Fig. 1(c) diffraction pattern shows characteristic peaks that correspond to AC and CS, as reported in previous

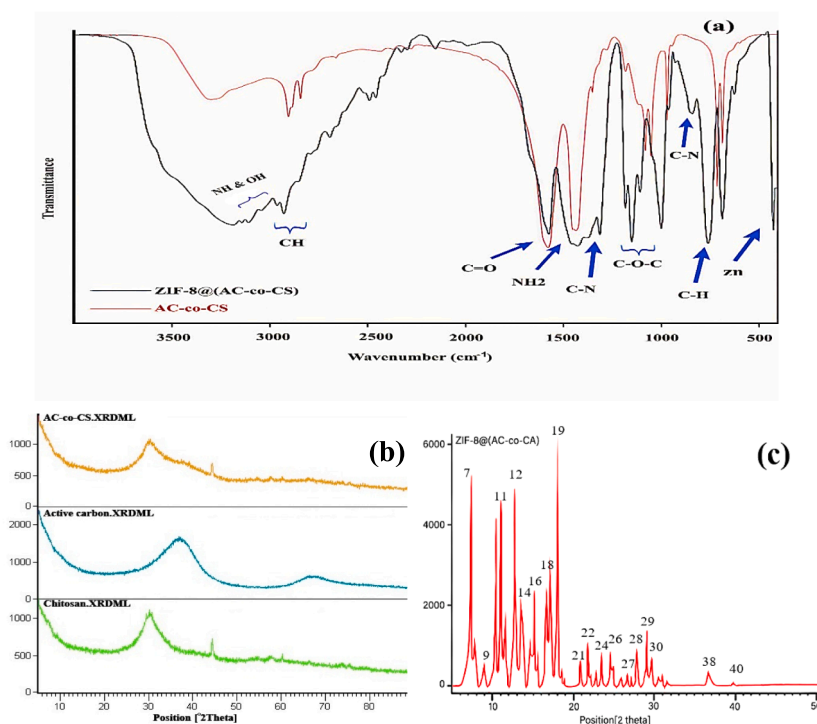


Fig. 1. (a) ATR-FTIR spectrum and (b), (c) XRD patterns of synthesized AC-co-CS and ZIF-8@(AC-co-CS) nanocomposite.

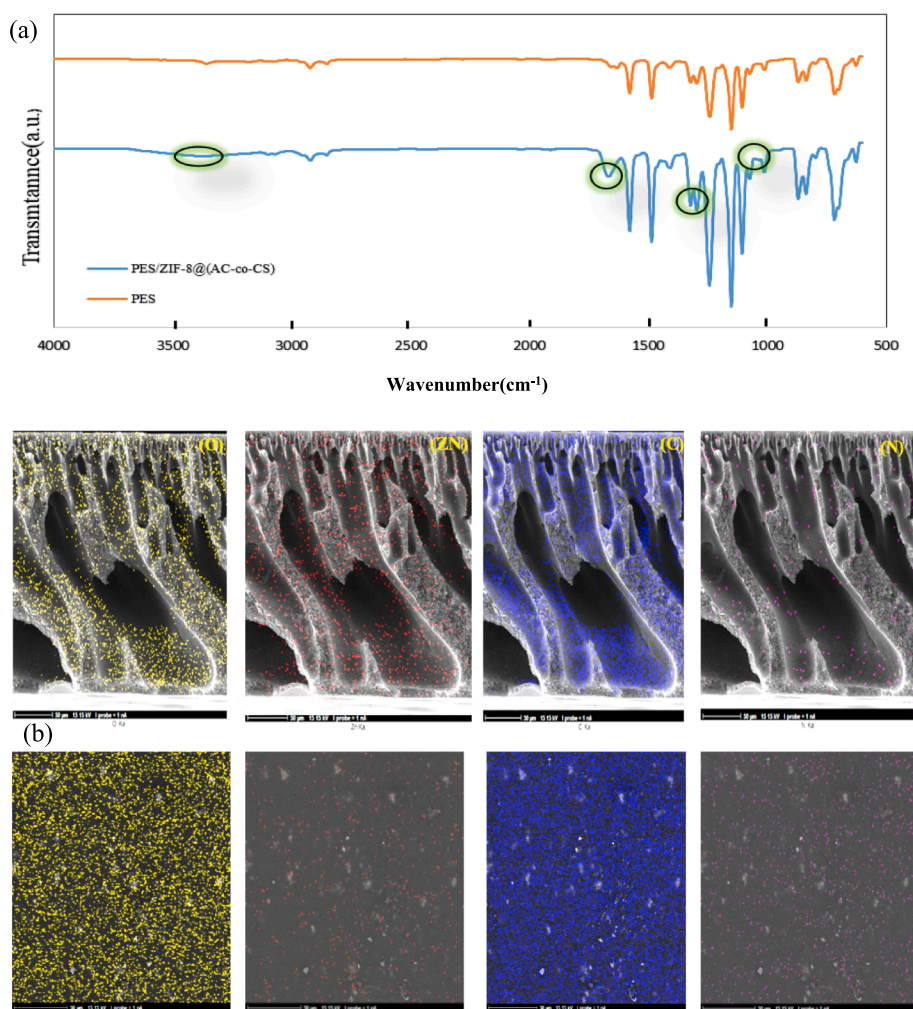


Fig. 3. (a) The ATR-FTIR spectra of the pristine and ZIF-8@(AC-co-CS) blended PES membranes; and (b) the surface and cross-sectional FESEM images along with MAP images of (O, Zn, N, and C) for the prepared membrane.

absorbed by the MMM. This occurrence has been corroborated by findings from previous studies (Halek et al., 2016, Ghiggi et al., 2017, Rezania et al., 2019). However, within the obtained spectrum of the modified membrane, a broad peak in the range of 3375 cm^{-1} has appeared, indicating the presence of an -OH bond in the membrane containing the ZIF8@(AC-co-CS) structure. Much like the PES membrane, the spectral bands in the MMM containing ZIF-8@(AC-co-CS) exhibit noticeable repetition. Nevertheless, we can infer the presence of ZIF-8@(AC-co-CS) within the membrane structures from the three analogous bands at 1662 , 1304 , and 1063 cm^{-1} . These findings are consistent with the results obtained from the ATR-FTIR analysis of ZIF-8@(AC-co-CS). After examining the ATR-FTIR outcomes, we received a MAP to ascertain the nanoparticle distribution within the membrane structure, as shown in Fig. 3(b). The examination revealed that the critical components of the nanoparticles, namely zinc, carbon, oxygen, and nitrogen, were evenly distributed across both the surface and cross-sectional areas of the MMM containing ZIF-8@(AC-co-CS).

Fig. 4 exhibits FESEM pictures portraying both the surface and cross-sectional membrane samples. Early examination of all images of FESEM shows that bare membranes and mixed matrix membranes all have an asymmetric structure containing a select at the top and a porous layer with a finger-link structure. As visible in the FESEM depiction of the PES membrane (MO), the separation layer exhibits substantial thickness, while the membrane's structure is dense. The MMMs containing ZIF-8@(AC-co-CS) exhibit greater porosity than PES membranes. Table 3

presents the results for porosity. Moreover, the hydrophilic nature of ZIF-8@(AC-co-CS) has enhanced the size and abundance of surface pores (Hosseini et al., 2020). Exchange rate fluctuations during the phase inversion process and the behavior of the casting solution primarily influence pore formation and porosity structure (Vatanpour et al., 2018, Khosravi et al., 2022). Furthermore, by adding 0.001, 0.005, and 0.01 wt% ZIF-8@(AC-co-CS) nanocomposite to the dope solution, which gives them stable mechanical strength, no flaw on the membrane was found (Seidyipoor et al., 2023). The migration of nanocomposites toward the membrane's surface results in a smooth surface that amplifies the rate at which solvent (DMAc) and non-solvent (water) interactions occur. Table 3 provides the roughness measurements of the membrane surfaces. This phenomenon accelerates the transfer of the non-solvent (water) mass through the membrane, resulting in an increased deposition rate of PES during membrane fabrication. In turn, it triggers instantaneous phase separation. The acceleration of a phase transition generates more channels and cavities (Karami et al., 2023). However, when incorporating 0.1 % and 1 % by weight of ZIF-8@(AC-co-CS) nanocomposite into the membranes, the nanoparticles begin to clump together, which slows down the phase change rate, the nanoparticles start to stick together more, which reduces the phase change rate. This leads to a denser membrane structure with less porosity, fewer cavities, and closed-end channels. As a result, a higher concentration of nanocomposite leads to a denser membrane structure, as shown in Table 3 (Mirzamohammadi et al., 2021). This study aimed to improve

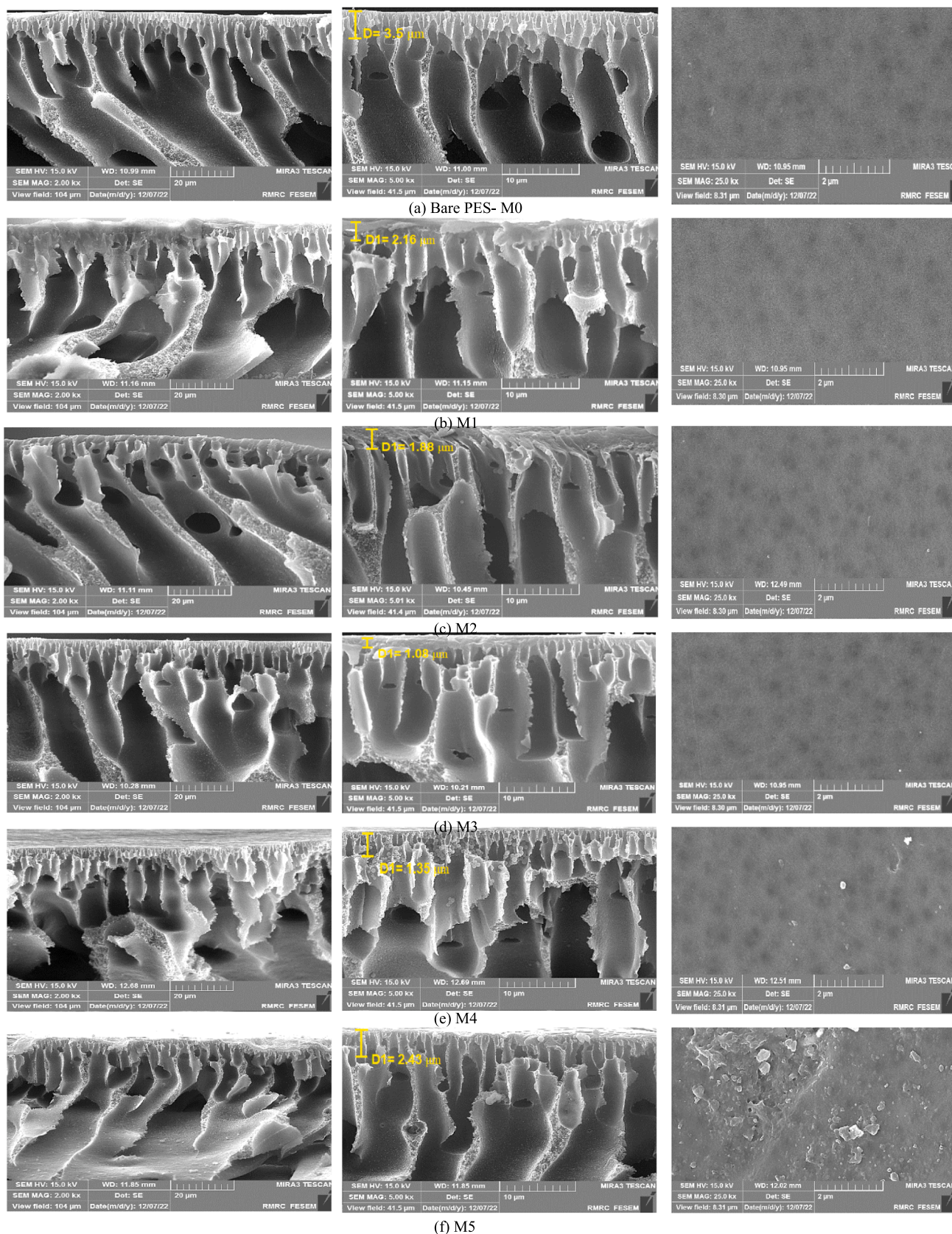


Fig. 4. Surface and cross-sectional FESEM images for the pristine and ZIF-8@(AC-co-CS)/PES membranes.

Table 3

Examining Membrane Parameters: Total Porosity, Average Pore Radius, and Roughness Surface Characteristics.

Name	Porosity (%)	Average pore size (nm)	Contact angle (°)	Roughness (nm)
Bare PES	64.2 ± 0.1	2.29 ± 0.4	61.4 ± 2.2	8.9
ZIF-8@(AC-co-CS) 0.001 wt%	71.8 ± 0.2	2.46 ± 0.6	58.14 ± 0.2	6.94
ZIF-8@(AC-co-CS) 0.005 wt%	72.3 ± 0.1	2.78 ± 1.1	53.31 ± 2.8	7.5
ZIF-8@(AC-co-CS) 0.01 wt%	75.9 ± 0.1	3.3 ± 0.2	51.1 ± 2.1	4.61
ZIF-8@(AC-co-CS) 0.1 wt%	69.8 ± 0.3	2.9 ± 0.5	46.4 ± 2.4	7.16
ZIF-8@(AC-co-CS) 1 wt%	67.8 ± 0.7	2.4 ± 1.5	42.17 ± 1.3	12.53

the effectiveness of a membrane in removing pollutants by introducing varying concentrations of ZIF-8@(AC-co-CS) nanocomposite in its structure. The results demonstrated that using ZIF-8@(AC-co-CS)/PES membranes increased water flux and lower contact angles, improving pollutant removal.

Table 3 presents the results of various tests on the prepared membranes, including water contact angle (WCA) and porosity. The property of hydrophilicity is connected to chemical structure and surface membrane geometry. The surface hydrophilicity of the membrane significantly affects its ability to allow substances to pass through while resisting fouling (Hosseini et al., 2019). Calculating the WCA is a widely used method for gauging the hydrophilicity of a membrane, where a lower WCA indicates higher surface wettability and hydrophilicity. To measure the hydrophilicity of the membrane surface, we used a contact angle measuring device to measure the contact angle between water and the membrane surface. The probe liquid used was deionized water, and the contact angle was measured three times for each sample under typical environmental conditions, with the resulting average angle being reported. The results indicated that the bare PES membrane had the highest WCA (61°), whereas incorporating 1 and 0.1 wt% ZIF-8@(AC-co-CS) in the membranes reduced the WCA to 46° and 42°, respectively. The hydrophilic nanocomposite migration to the membrane surface through the phase inversion operation could cause a decrease in WCA. The ZIF-8@(AC-co-CS) nanocomposite contains oxygen-containing functional groups (–COOH and –OH) that attract water molecules through strong hydrogen bonding (Cohen-Tanugi and Grossman 2012). Additionally, these functional groups on the ZIF-8@(AC-co-CS)/PES membrane play a crucial role in its water flux. Their high capacity for water uptake enhances the membrane's hydrophilicity, leading to increased water flux even under low operating pressures. Other studies have reported that incorporating CS reduces the WCA and improves the membrane's hydrophilic surface (Ganji et al., 2022, Salehi et al., 2022, Khoerunnisa et al., 2023).

In Table 3, all MMMs containing ZIF-8@(AC-co-CS) exhibited larger pores than MO. This could be attributed to the increased membrane heterogeneity caused by the presence of ZIF-8@(AC-co-CS) nanocomposites. Furthermore, the heightened surface energy and efficient dispersal attributes of the nanocomposites within the membrane structure potentially change the exchange rate. During the phase change, interactions between the polymer solution and water molecules lead to the formation of pores with larger diameters (Kali et al., 2023). The improved separation performance observed in the MMMs containing 0.01 wt% ZIF-8@(AC-co-CS) compared to the MMMs containing 0.001 wt% and 0.005 wt% ZIF-8@(AC-co-CS) can be attributed to the higher concentration of nanocomposites in the casting solution, which increases the hydrophilicity and water diffusion rate (non-solvent) into the developing membrane during the phase inversion process. However, incorporating ZIF-8@(AC-co-CS) nanocomposite at 0.1 wt% and 1 wt% into the PES membrane resulted in a noticeable decrease in both the overall porosity and water flux of the blended membranes. This

phenomenon can be attributed to the pores-filling effect caused by the nanocomposites, which reduces both membrane porosity. Fig. 5 illustrates 2D and 3D AFM pictures of both pristine and MMMs containing ZIF-8@(AC-co-CS). Loading ZIF-8@(AC-co-CS) into the neat membrane matrix decreases surface roughness (see Table 3). The ZIF-8@(AC-co-CS) nanocomposite approaching the MMM surface generates noticeable peaks and valleys at substantial intervals. The surface roughness of the MMMs containing 0.001 and 0.005 wt% of ZIF-8@(AC-co-CS) nanocomposite was decreased to 6.9 nm and 7.5 nm. increasing the quantity of ZIF-8@(AC-co-CS) in the MMM up to 0.01 wt% results in a smoother surface with peaks and valleys evenly spaced apart and reduces the surface roughness to 4.6 nm. This could be attributed to potential electrostatic interactions between PES chains and NH₂ groups. Nevertheless, increasing the ZIF-8@(AC-co-CS) concentration to 0.1 % and 1 % by weight leads to a more significant accumulation of the nanocomposite material on the MMM surface. This accumulation leads to a rougher surface. Nevertheless, according to reports, the effects of functional groups resulting from the increase in the number of amines and hydroxyl groups on the membrane surface prevail over the surface roughness effects, increasing hydrophilicity.

Table 4 displays the zeta potential values for the unmodified membrane and membranes blended with ZIF-8@(AC-co-CS). The pH range of the contaminants specified in Table 1 is 6–7, during which all membranes exhibit a negative zeta potential. The presence of the ZIF-8@(AC-co-CS) nanocomposite increases the negative charge on the modified membrane's surface due to the hydroxyl and carboxyl groups. This increase in negative charge occurs because of the deprotonation of these groups in an aqueous environment (Sahu et al., 2023). The surface charge of pollutants such as dyes can vary depending on the solution pH. Dyes can have positive, negative, or neutral charges at different pH levels. Similarly, many metal ions have a positive charge. As a result, the more excellent opposing surface electrical charge of the entire nanocomposite membrane, combined with the specific surface charges of the contaminants, leads to improved removal efficiency due to electrostatic interactions (Dutta et al., 2021, El-habacha et al., 2023, Cigeroglu et al., 2024).

3.3. Mixed matrix membrane efficiency

3.3.1. Permeability, separation ability, and surface hydrophilicity

This study investigated the efficacy of membranes in filtering various substances using a dead-end filtration system. We carefully considered parameters such as permeability and separation ability. The performance of the membranes was assessed by measuring factors including PWF, rejection, and removal efficiency for different materials. Subsequently, the membranes underwent compression at a specific pressure for 15 min after the experiments. During the filtration tests, we applied a pressure of 0.45 MPa for 60 min. The results unveiled a direct correlation between PWF and the surface's hydrophilic properties, consistent with findings from prior studies (Zareei and Hosseini 2019). Additionally, Fig. 6 showed that the trend of PWF corresponded well with the hydrophilic properties, total porosity, and average pore size of the membranes. The study found that the PWF of the neat PES membrane was initially 8 L/m².h, but with adding 0.01 wt% of ZIF-8@(AC-co-CS) nanocomposites, it increased significantly to 28 L/m².h. This is attributed to the abundance of amine groups in the ZIF-8@(AC-co-CS) structure, which increases the membrane's surface hydrophilicity and mean pore size and porosity. However, for the MMMs containing 0.1 and 1 wt % of the nanocomposite, the pure water flux decreased to 21 L/m².h and 19 L/m².h, respectively. As mentioned earlier, this decrease is attributed to the reduction in the average pore size of the MMMs, the denser MMMs structure, and the presence of closed-end channels. These results of the FRR are illustrated in Fig. 6.

3.3.2. Anti-fouling performances of different the MMM

Membrane fouling is a critical issue in membrane filtration that can

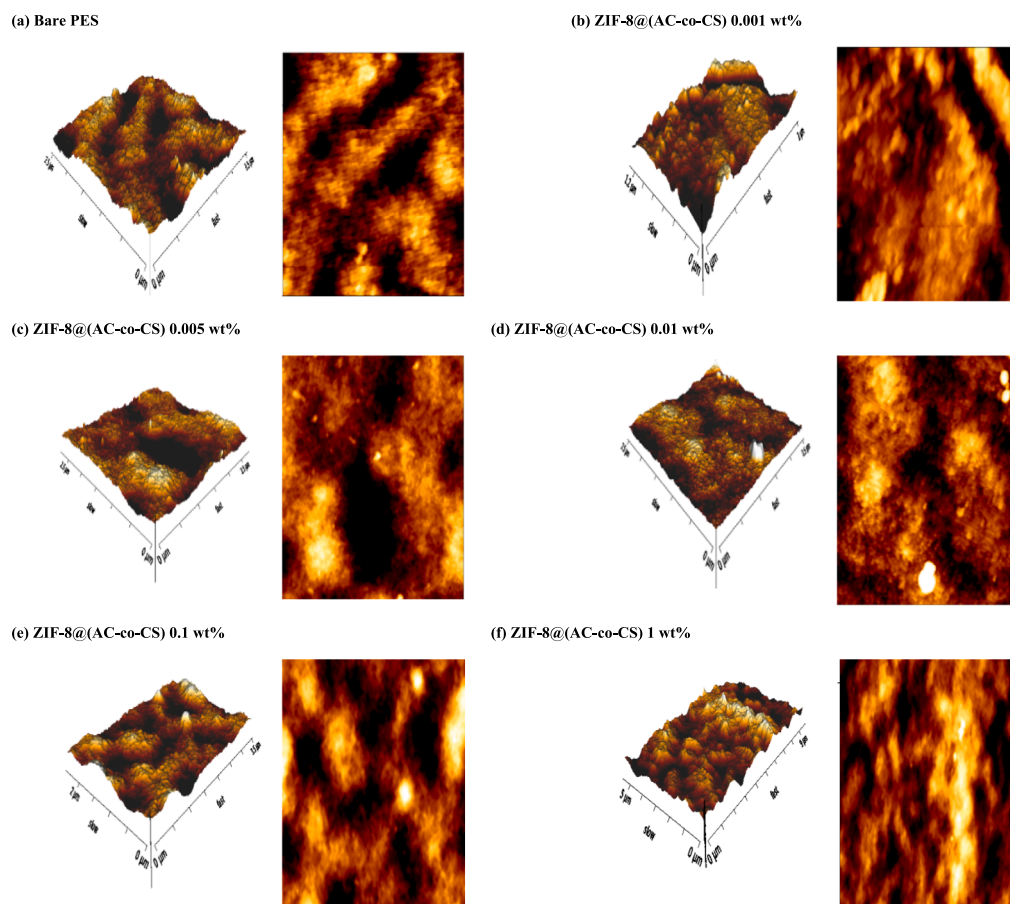


Fig. 5. The AFM images depict the prepared membranes.

Table 4

Comparing Zeta Potential of unmodified and ZIF-8@(AC-co-CS) blended membranes.

Zeta Potential (mV)		
pH	Bare PES	ZIF-8@(AC-co-CS)/PES
3	-0.34	1.53
4	-3.11	-3.46
6	-4.04	-4.92
7	-5.17	-6.59
8	-8.59	-9.87
10	-11.85	-15.53

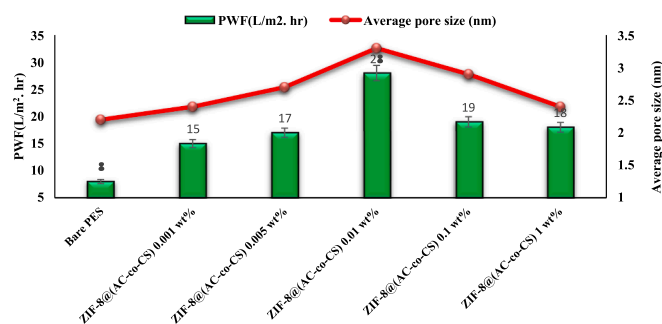


Fig. 6. The assessed pure water flux and average pore size for the produced membrane.

significantly impact the performance of the membrane. It reduces the lifespan of the membrane, increases washing costs, and decreases filtration efficiency. Addressing membrane fouling is a crucial aspect of separation and filtration that relies on membranes (Du et al., 2023). One potential solution to the membrane fouling problem is the incorporation of hydrophilic nanofillers into the membrane, as suggested by other researchers (Wang et al., 2022). To evaluate the performance of modified membranes, various substances, including milk powder solutions, are used (Bagheripour et al., 2018, Farahani and Hosseini 2022, Khosravi et al., 2022). In one experiment, we added a milk powder solution with a concentration of 250 ppm to the membrane cell after measuring the water permeation for 60 min. We assessed the permeate flux for an additional hour before washing the fouled membrane. Then, the washed membrane was tested for another hour to measure the pure water flux again. Fig. 7(a) presents the results, demonstrating a decrease in water permeability following the introduction of the milk powder solution, followed by an increase after replacing the fouled solution with pure water. This pattern occurs due to the elimination of reversible fouling following membrane cleaning. In this study, we utilized the unique characteristics of AC-co-CS composite nanoparticles to enhance the surface area of ZIF-8. As a result, the ZIF-8@(AC-co-CS) nanocomposites exhibited an improved surface area. This feature traps foulant particles within the branches of the material and prevents them from passing through the membrane. It is difficult to avoid this issue despite forming a protein layer on the surface of the membrane through surface interaction. However, it is possible to alter the composition of this layer by incorporating nanoparticles into the matrix of the membrane and, or modifying the surface of the membrane. These alterations result in multiple active minutiae surrounding the particle, which reduces the passage of protein molecules and enhances their interaction.

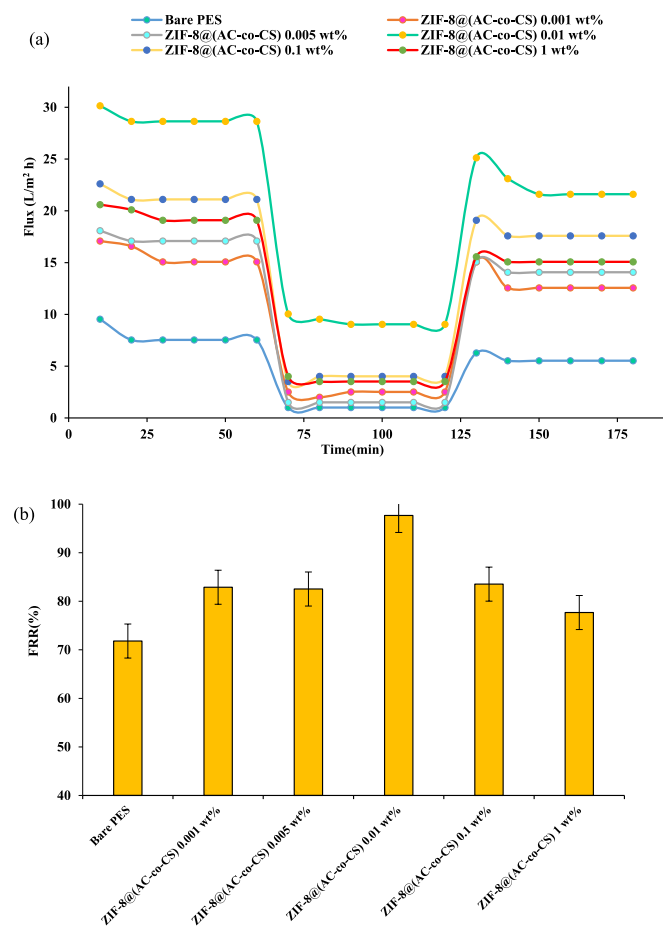


Fig. 7. (a) The Membrane's Combined Performance in Water Permeation, Protein Solution Flux, Subsequent Pure Water, and (b) Flux Recovery Rate (FRR) in the fabricated PES membrane.

Consequently, this helps to reduce the flux recovery ratio. The result was previously reported in the literature [12].

As seen in Fig. 7(a) and Table 5, the modified MMMs generally demonstrated improved permeance flux compared to the PES membrane matrix. Among all the modified membranes, the membrane containing 0.01 wt% of ZIF-8@(AC-co-CS) nanocomposites showed better permeance flux. Enhancing permeability of the membrane relies on its hydrophilicity and smooth surface.

The degree of FRR is a crucial factor in evaluating membrane anti-fouling properties (Amiri et al., 2023). The calculated FRR for the prepared membranes is presented in Fig. 7(b). According to the results, the FRR for the pure PES membrane was 52 %, so it has fragile anti-fouling properties compared to the modified MMMs. In this case, adding ZIF-8@(AC-co-CS) nanocomposite up to 0.01 wt% increased the FRR parameter. The benefit can be explained by the unique properties of ZIF-8@(AC-co-CS) nanocomposites, which include regular and hyperbranched structures, porous spaces, and macromolecule features. These properties

Table 5

The amount of flux for the prepared membrane: Water Permeation(J_{w1}), Protein Solution Flux(J_p), and Pure Water Flux for the clean membrane(J_{w2}).

Name	J_{w1}	J_p	J_{w2}
Bare PES	8	1	5
ZIF-8@(AC-co-CS) 0.001 wt%	15	2	13
ZIF-8@(AC-co-CS) 0.005 wt%	17	1	14
ZIF-8@(AC-co-CS) 0.01 wt%	28	9	22
ZIF-8@(AC-co-CS) 0.1 wt%	21	4	18
ZIF-8@(AC-co-CS) 1 wt%	19	5	15

promote surface coverage and enhance the overall performance of the membrane. Furthermore, as previously discussed, this phenomenon may be attributed to the improvement in separation properties and the chemical and physical performance of the membrane, such as surface hydrophilicity and surface roughness. The decrease of FRR at high nanocomposite concentrations may be due to increased surface roughness and the aggregation of nanocomposites that would promote concentration polarization on the membrane surface.

Additionally, when evaluating the anti-fouling attributes of membranes, other parameters such as R_t , R_p , and irreversible fouling are commonly considered (Moradi et al., 2023, Samari et al., 2024). Fig. 8 (a) depicts the recorded R_t , R_p , and R_{ir} values for both the unmodified and modified membranes. R_t originates from concentration polarization and the buildup of fouling particles on the surface of the membrane, a condition readily remedied through washing. Conversely, irreversible fouling results from the permanent adhesion of fouling-agent particles within the membrane's pores and along its surface, resisting easy removal through washing [45, 46]. The introduction of ZIF-8@(AC-co-CS) at a concentration of 0.01 wt% displayed a higher (R_t/R_{ir}) ratio. This phenomenon can be attributed to the increased hydrophilic nature of the nanocomposite membrane, resulting from the presence of hydroxyl and amine groups within the AC-co-CS structure. Conversely, protonated terminal groups and the surface of AC-co-CS are active locations for chemical bonding, generating an increased surface charge of the nanocomposite membrane (Mohammadifakhr et al., 2020). As a result, incorporating them into the framework of the ZIF-8 structure has yielded favorable outcomes, as evidenced by the reduction in WCA and enhancement in porosity upon introducing these nanocomposites into the casting solution. Water molecules are more likely to adsorb onto membranes with higher surface hydrophilicity. These accumulated water molecules form a protective layer that hinders the foulant deposition on the membrane surface. As illustrated in Fig. 8(b), the amounts of R_t , R_p , and R_c exhibited a substantial reduction in the 0.01 wt% ZIF-8@(AC-co-CS) nanocomposite membrane compared to the unmodified membrane. They were notably lower than those observed in other modified membranes. The compressibility of the cake layer depends on operational parameters such as volume, duration, surface flux, pressure, and surface area (Bian et al., 2022). A denser cake layer reduces porosity and enhances the resistance of the pores to water flow, leading to decreased fluid permeation (Szczęśniak et al., 2018, Nasrollahi et al., 2019). The cake resistance plays a crucial role in membrane separation processes, influencing both the longevity and efficiency of the membrane.

3.3.3. Flux stability in salt solution separation

To assess the stability of flux during salt solution separation, we repeated the flux experiment multiple times and evaluated the results. The purpose of these experiments was to measure the membranes' ability to consistently maintain a high flux rate over an extended period. For this study, we conducted six flux experiments on the modified membrane, labeled as experiments 1 through 6. For the flux measurements for each experiment, we recorded the results as follows: 27.4, 26.6, 25.4, 25.5, 26.2, and 26.7 L/m²·h, respectively. The results showed a relatively consistent flux for this sample throughout the filtration experiment, which is due to its strong recovery capability.

3.3.4. Performance of membrane separation

The research evaluated the effectiveness of both unmodified and modified membranes in removing various substances, including Na₂SO₄ and MgSO₄ salt solutions, dyes, and heavy metals. The separation efficiency of the modified membranes is illustrated in Fig. 9, showing their effectiveness in removing various types of contaminants. The primary mechanisms contributing to membrane rejection include Donnan exclusion, sieving, hydrophobic interactions, adsorption, and solute dehydration (Gao et al., 2023, Nellur et al., 2023). Charge-dependent separation results from the Donnan effect of electrostatic phenomena

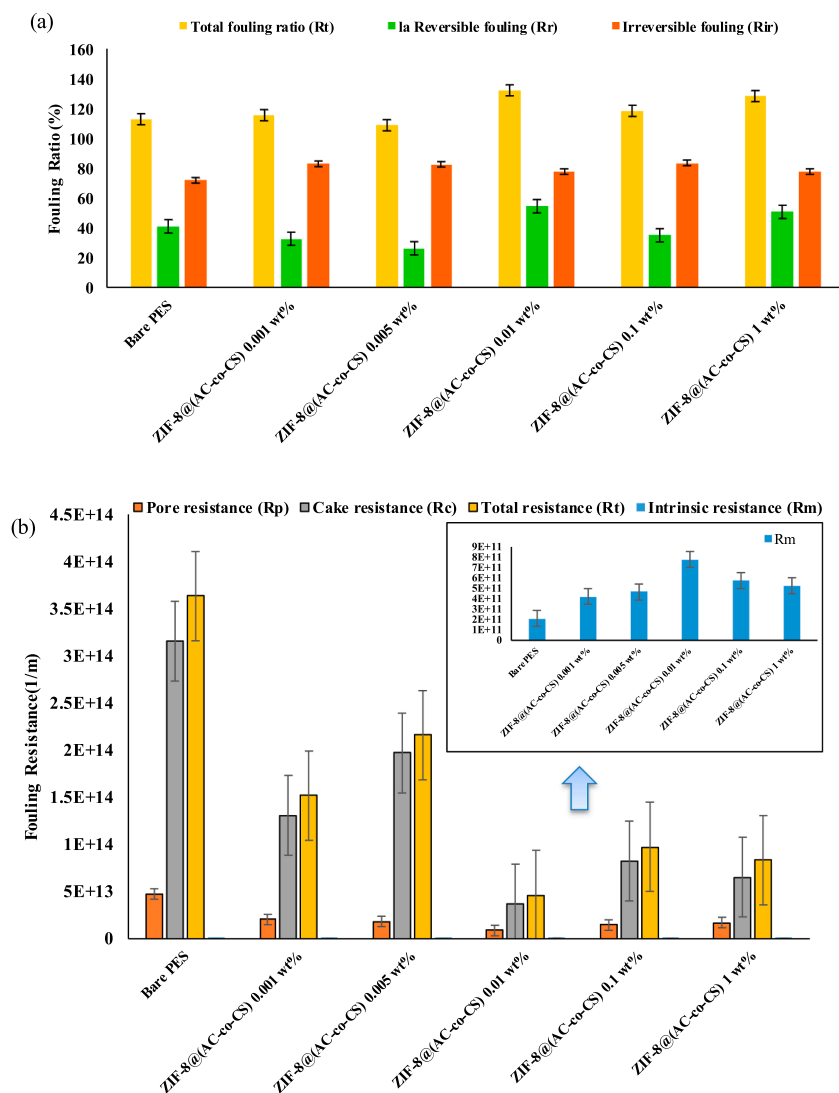


Fig. 8. (a) Fouling ratio and (b) Membrane Fouling Resistance Parameters.

(Naik et al., 2021, Sun et al., 2023), while size-dependent separation occurs through a sieving mechanism. (Zhang et al., 2023). Fig. 9(a) illustrates the outcomes of the separation process for salts such as Na_2SO_4 and MgSO_4 . The rejection sequence for all membranes followed the pattern $\text{Na}_2\text{SO}_4 > \text{MgSO}_4$, which corresponded well with the typical rejection sequence observed in negatively charged nanofiltration membranes. Among the prepared membranes, the PES membrane exhibited the least effective separation performance because, in its structure, there are no sites for either excretion or adsorption. The ZIF-8@(AC-co-CS) 0.01 wt% membrane exhibited rejections of 96 % for Na_2SO_4 and 89 % for MgSO_4 . This membrane, with larger pores and a thinner separation layer than other membranes, demonstrated superior separation efficiency. The results for the thickness of the separation layer are presented in Fig. 4. Furthermore, the enhanced salt rejection is primarily attributed to Donnan exclusion facilitated by the negative charge of the ZIF-8@(AC-co-CS) 0.01 wt% membrane (as provided in Table 4). The modified membranes, incorporating ZIF-8, AC, and CS, exhibit enhanced adsorption properties, potentially leading to increased selective adsorption of divalent salts and higher retention than the bare membrane (Gowribooy et al., 2022, Sharma et al., 2023). The presence of amine functional groups on the nanocomposite surface introduces a negative charge and free electron pairs from nitrogen. This enhances the interaction between divalent ions and the membrane surface, leading to a stronger attraction for Mg ions than Na ions (Gao et al., 2022, Moradi

et al., 2022). Additionally, divalent ions can poison the surface functional groups of the membrane due to their strong interactions. Consequently, the probability of penetration through the membrane increases, and selectivity decreases. This results in a reduction in the efficiency of separation for Mg cations compared to Na cations. However, the decreased salt rejection observed in ZIF-8@(AC-co-CS) 0.1 wt% and ZIF-8@(AC-co-CS) 1 wt% membrane could be attributed to the aggregation of nanoparticles at elevated additive concentrations, falling below their adsorption capacity. In addition, the formation of cracks within the membrane matrix may contribute to this decline in rejection, leading to a decrease in salt rejection. The discharge of heavy metals is a significant environmental concern that can lead to various illnesses and pose risks to human health. Fig. 9(a) depicts an analysis of the rejection of solutions containing CrSO_4 and CuSO_4 . The key factor contributing to the increased rejection is the adsorption mechanism triggered by the saturation of membrane adsorption sites due to adsorbed Cr^{2+} and Cu^{2+} metal ions on the membrane surface. For all the fabricated membranes, the order of rejection was $\text{Cr}^{2+} > \text{Cu}^{2+}$. As shown in Fig. 9(a) the ZIF-8@(AC-co-CS) 0.01 wt% membrane exhibited the highest efficiency in separating and removing CrSO_4 (96.04 %) and CuSO_4 (94.36 %), compared to the bare membrane, which only achieved 62 % and 55 % removal, respectively. This improvement results from nitrogen and oxygen atoms in the amine, carboxyl, and hydroxyl end groups within ZIF-8@(AC-co-CS). Additionally, the synergy of a negatively charged

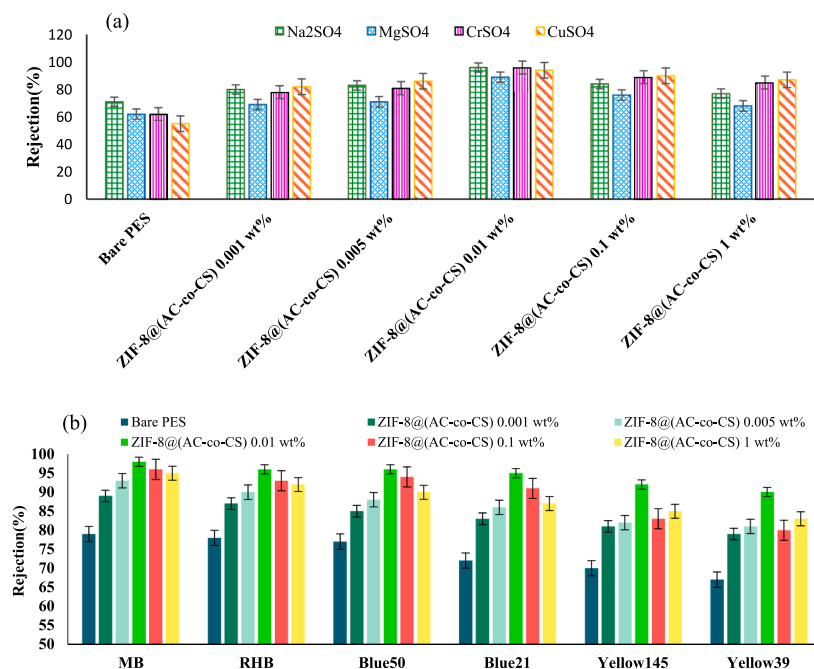


Fig. 9. (a) Salt solutions retention and (b) the results of dye rejection for the prepared MMMs.

membrane surface and the effective adsorption of nanostructures play a crucial role in excluding heavy metal ions through electrostatic interaction (see Table 4) (Zareei et al., 2021). This mechanism leads to the rejection of these ions. However, the marginal decrease in heavy metal ion rejection in the ZIF-8@(AC-co-CS) 0.1 wt% and 1 wt% membrane compared to the ZIF-8@(AC-co-CS) 0.01 wt% membrane can be attributed to the aggregation of nanocomposites at higher concentrations of ZIF-8@(AC-co-CS) within the membrane structure and available adsorption sites of the nanocomposites. Typically, the removal efficiency of ions increases when the co-ion possesses a higher valence and a larger hydrated radius, as these factors contribute to heightened repulsion between ions. Moreover, a high hydrated radius coupled with a low ionic radius leads to diminished ion diffusion into the nanocomposites and membrane surface. Consequently, Cr^{2+} , with its larger hydrated radius and smaller ionic radius, exhibits a higher capacity for removal than Cu^{2+} . This disparity can be attributed to the effects of steric hindrance and the difficulty of ions passing through the nanocomposites (Bandeali et al., 2019; Seidyipoor et al., 2023).

The results depicted in Fig. 9(b) illustrate the removal percentage for different dyes. The primary factors influencing separation in nanofiltration systems are the charge and size of the particles or molecules involved. These mechanisms play pivotal roles in the ability of the membrane to reject various substances and facilitate the purification process. This membrane demonstrated superior separation efficiency due to its larger pores and thinner separation layer compared to other membranes. Filtration experiments were conducted using solutions of MB, RhB, and reactive dyes, including RY39, RY145, RB21, and RB50, each at a concentration of 20 ppm. These experiments were performed at room temperature and a pressure of 4.5 bar. The dye rejection outcomes for the composite membranes are displayed in Fig. 9(b). The figure demonstrates that the enhanced ZIF-8@(AC-co-CS) membrane exhibited an elimination efficiency ranging from 67% to 97% for MB, RhB, and all four reactive dyes, underscoring its superior performance. Furthermore, the improved effectiveness of the modified membranes in eliminating pollutants may be attributed to electrostatic repulsion between the negatively charged membranes and the reactive anionic dyes, all four of which are negatively charged, particularly under normal pH conditions. The zeta potential of the modified membrane, measured at pH 7, was found to be -6.59 . Enhancing the hydrophilicity of the membrane also

tended to facilitate the diffusion of water molecules while inhibiting the diffusion of polar organic compounds, such as dyes. The removal efficiency for methyl blue and Rhodamine B dyes was superior to all reactive dyes. We assessed the best membrane for its ability to remove various dyes. The membrane containing 0.01 wt% nanocomposites performed best in removal efficiency and flux for reactive blue 50 and 21, the former due to its lower molecular weight and the latter for its higher molecular weight compared to other reactive anionic dyes with similar molecular weight. This indicates that the capacity of the membrane to filter dyes is influenced by both molecular weight and chemical structure. Furthermore, the shape of the dyes was noted to play a crucial role in determining both the percentage of removal and the passing flux. Specifically, spherical dyes demonstrated higher removal efficiency compared to dyes with a straight structure (Khosravi et al., 2022). So, in contrast, RB21 and RB50 have spherical structures, while RY39 and RY145 have bar structures, exhibiting a lower degree of removal capability. The composite membrane containing 0.01 wt% nanocomposites showed the highest dye retention, with rates of 97.8% for MB, 96.2% for RhB, 94.6% for RB50, 91% for RB21, 89.8% for RY145, and 86.7% for RY39. It is important to note that as the concentration of ZIF-8@(AC-co-CS) nanocomposite in the membrane structure increased from 0.1% to 1%, the rejection of the studied dyes decreased. This decrease was likely due to changes in surface charge and pore size.

4. Comparison with other literature

A summary of different research studies investigating the removal of contaminants such as dye, heavy metals, and salt is presented in Table 6. These studies, including the current research, indicate that incorporating hydrophilic nanoparticles into the PES membrane matrix is a highly effective approach for reducing these pollutants. Moreover, the results of this study provide evidence that enhancing the PES membrane through the utilization of MOF and nanostructure methods can significantly improve its performance in pollutant removal. The modified PES membrane exhibited a removal efficiency exceeding 80% for salts and over 90% for heavy metals and reactive dyes. Table 6 compares the separation efficiency of the ZIF-8@(AC-co-CS)/PES membrane with those reported in some recently published articles. The data show that the membrane synthesized in this study achieved the highest rejection

Table 6

Performance Comparison: ZIF-8@(AC-co-CS)/PES membrane vs. reported results.

Polymer and Concentration (wt %)	Membrane type	Additive	Solute rejected (%)	Ref
PES20	NF	PAA-MWCNT 0.1 wt%	Na ₂ SO ₄ :93.20 NaCl: 40.56	(Daraei et al., 2013)
PES20	NF	Tannin acid/ boehmite	Direct Red 16: >96	(Zhang et al., 2014)
PES21	NF	GO/TiO ₂ 0.1 wt%	Green 19:95.50 Yellow 12:93.30 Blue 21:79.72	(Safarpour et al., 2016)
PES 21	NF	NH ₂ -MWCNT	Na ₂ SO ₄ :36.71 NaCl:95.72	(Zinadini et al., 2017)
PES21	NF	NCDs	Na ₂ SO ₄ :80.3 MgSO ₄ :63.5 NaCl:20.7 RR198: > 99.2	(Wang et al., 2017)
PES15	UFended	ZIF-8@MXene	Na ₂ SO ₄ :10 Rhodamine B:98	(Yao et al., 2022)
PES20	NF	amine-functionalized boron nitride 1 wt%	Reactive Blue 19:>99	(Vatanpour et al., 2020)
PES20	NF	PVA-GO-NaAlg 1 wt%	Lanasol blue 3R:88.90	(Amiri et al., 2020)
PES20	NF	Fe ₃ O ₄ @SiO ₂ -CS	Na ₂ SO ₄ :97.75 Methylene Blue:38.25	(Kamari and Shahbazi 2021)
PES18	NF	Uio-66-NH ₂ 0.01 wt%	Na ₂ SO ₄ :93.20 MgSO ₄ :89.27 NaCl: 40.56 MgCl ₂ :52.5 Blue 21:83.60 Rhodamine B:94.20	(Farahani and Hosseini 2022)
PES20	NF	Cu-MOF@CA	HA:79 BSA:85	(Gowriboy et al., 2022)
PES21	NF	Mil-Den 0.2 wt%	Na ₂ SO ₄ :65.21 Pb(NO ₃) ₂ : 97.36 Cefixime:80.04 Green 19:99.31 Blue 50:85.18 Blue 21:98.20 Yellow 145:94.67 Yellow 160:82.49 Yellow 39:79.05	(Khosravi et al., 2022)
PES 18	NF	Cu ₂ O	Na ₂ SO ₄ :66.94 Pb(NO ₃) ₂ :85.08 CrSO ₄ :79.38 Cu(NO ₃) ₂ :81	(Moghaddasi et al., 2023)
PES 18	NF	Fumarate-alumoxane	Direct red 16: 99	(Moradi et al., 2023)
PES	NF	UiO-66-NH ₂	Reactive Blue 50: 98.5	(Yu et al., 2024)
PES	NF	Ag/Cu	Pb(II):92.6 reactive black 5:96.4 reactive red:98.4	(Vatanpour et al., 2024)
PES18	NF	ZIF-8@(AC-co-CS) 0.01wt%	Na ₂ SO ₄ :96.85 MgSO ₄ :86.05 CrSO ₄ : 97.50 Cu(NO ₃) ₂ :94.30 Blue 50:92.20 Blue 21:94.89 Yellow 145:89.49 Yellow 39:86.05 Rhodamine B:95.18 Methylene Blue:97.33	This work

rates for various contaminants, including MB, RhB, RB50, RB21, RY145, RY39, Na₂SO₄, MgSO₄, CrSO₄, and CuSO₄, among different MMMs. The specific solute rejection rates were 96.85 % for Na₂SO₄, 86.05 % for MgSO₄, 97.50 % for CrSO₄, and 96.30 % for CuSO₄. This performance improvement is attributed to incorporating the ZIF-8@(AC-co-CS) nanocomposite. The exceptionally high separation efficiency of the ZIF-8@(AC-co-CS)/PES membrane, compared to similar membranes, underscores its cost-effectiveness in filtration processes.

5. Conclusion

This study prepared a new nanocomposite ZIF-8@AC-co-CS/PES membrane for water treatment. The ZIF-8@(AC-co-CS) nanocomposite was synthesized using a co-precipitation method and examined using FTIR, FESEM, and XRD analyses. These analyses confirm that the nanocomposite, ZIF-8@(AC-co-CS), was synthesized with uniform size.

FTIR and XRD decisively confirm the formation of ZIF-8@(AC-co-CS). PES/ZIF-8@(AC-co-CS) membrane properties were also investigated by FESEM, porosity analysis, water content measurement, roughness assessment, water contact angle measurement, flux evaluation, separation efficiency testing, and fouling analysis. The investigation outcomes revealed that the modified membranes led to enhanced hydrophilicity. According to the results, the ZIF-8@(AC-co-CS) nanocomposite was included due to the NH₂ and hydroxyl groups present in its unique structure, improving the hydrophilicity of the membrane. Using a combination of AC and CS in modifying ZIF-8 structures facilitated the creation of active sites with a strong affinity to interact with metal ions, enabling effective contaminant removal. The results obtained from FESEM and AFM analyses indicated significant increases in permeability compared to the pristine membrane. Incorporating the nanocomposite into the casting solutions enhanced total porosity, Mean pore diameter, and permeability. Notably, the MMM containing 0.01 wt% of ZIF-8@

(AC-co-CS) demonstrated a substantial increase in water permeability, reaching three and half times that of the virgin PES membrane. Additionally, the outcome showed that the membrane with 0.01 wt% ZIF-8@ (AC-co-CS) displayed superior performance in removing various contaminants. The surface roughness of the blended membrane containing 0.01 wt% ZIF-8@ (AC-co-CS) nanoparticles was nearly half that of the pristine membrane. The WCA of the membrane was also reduced from 61.4° to 42.17° using ZIF-8@ (AC-co-CS) nanocomposite. The antifouling results demonstrated that introducing the modified additives to the membrane significantly increased the flux recovery ratio (FRR) from 71 % to 97 % compared to the unmodified membrane. Rejection measured 97 % for MB, 96.2 % for RhB, 94.6 % for RB50, 91 % for RB21, 89.8 % for RY145, and 86.7 % for RY39, 96.85 % for Na₂SO₄, 86.05 % for MgSO₄, 97.50 % for CrSO₄, and 96.30 % for CuSO₄. Furthermore, MMMs exhibit enhanced rejection of cationic dyes compared to anionic dyes. This finding suggests that the blended ZIF-8@ (AC-co-CS)/PES-based membranes have great promise for water treatment applications. The ZIF-8@ (AC-co-CS)/PES-based membrane is a modified membrane that offers promising application fields and prospects. Its excellent filtration properties, selective permeation of gases, biocompatibility, and potential uses in water treatment, gas separation, biomedical engineering, and energy storage make it a versatile and valuable material. As research and development continue, it is anticipated that the ZIF-8@ (AC-co-CS)/PES-based membrane will find even more applications in various fields, contributing to advancements in technology, medicine, and environmental sustainability.

CRedit authorship contribution statement

Mina Afshari: Conceptualization, Formal analysis, Investigation, Methodology, Validation, Writing – original draft. **Abdolreza Moghadassi:** Conceptualization, Methodology, Project administration, Supervision. **Sayed Mohsen Hosseini:** Conceptualization, Methodology, Project administration, Supervision, Writing – review & editing.

Declaration of competing interest

The authors declare that they have no known competing financial interests or personal relationships that could have appeared to influence the work reported in this paper.

References

- Abid, Z., Abbas, A., Mahmood, A., et al., 2022. Water treatment using high performance antifouling ultrafiltration polyether sulfone membranes incorporated with activated carbon. *Polymers* 14, 2264.
- Ahmad, S.Z.N., Salleh, W.N.W., Yusop, M.Z.M., et al., 2023. Graphene oxide/zeolitic imidazolate framework-8 nanocomposite for lead ion removal. *Mater. Today: Proc.*
- Alenazi, N.A., Hussein, M.A., Alamry, K.A., et al., 2017. Modified polyether-sulfone membrane: a mini review. *Des. Monomers Polym.* 20, 532–546.
- Al-Hazmi, G., El-Bindary, M., El-Desouky, M., et al., 2022. Efficient adsorptive removal of industrial dye from aqueous solution by synthesized zeolitic imidazolate framework-8 loaded date seed activated carbon and statistical physics modeling. *Desalin. Water Treat.* 258, 85–103.
- Amiri, S., Asghari, A., Vatanpour, V., et al., 2020. Fabrication and characterization of a novel polyvinyl alcohol-graphene oxide-sodium alginate nanocomposite hydrogel blended PES nanofiltration membrane for improved water purification. *Sep. Purif. Technol.* 250, 117216.
- Amiri, S., Asghari, A., Vatanpour, V., et al., 2021. Fabrication of chitosan-aminopropylsilane graphene oxide nanocomposite hydrogel embedded PES membrane for improved filtration performance and lead separation. *J. Environ. Manage.* 294, 112918.
- Amiri, S., Vatanpour, V., He, T., 2023. Antifouling thin-film nanocomposite NF membrane with polyvinyl alcohol-sodium alginate-graphene oxide nanocomposite hydrogel coated layer for As (III) removal. *Chemosphere* 322, 138159.
- Bagheripour, E., Moghadassi, A., Hosseini, S., et al., 2018a. Highly hydrophilic and antifouling nanofiltration membrane incorporated with water-dispersible composite activated carbon/chitosan nanoparticles. *Chem. Eng. Res. Des.* 132, 812–821.
- Bagheripour, E., Moghadassi, A., Hosseini, S., et al., 2018b. Novel composite graphene oxide/chitosan nanoplates incorporated into PES based nanofiltration membrane: chromium removal and antifouling enhancement. *J. Ind. Eng. Chem.* 62, 311–320.

- Bahador, F., Foroutan, R., Esmaeili, H., et al., 2021. Enhancement of the chromium removal behavior of *Moringa oleifera* activated carbon by chitosan and iron oxide nanoparticles from water. *Carbohydr. Polym.* 251, 117085.
- Bandeali, S., Moghadassi, A., Parvizian, F., et al., 2019. A new type of [PEI-glycidyl POSS] nanofiltration membrane with enhanced separation and antifouling performance. *Korean J. Chem. Eng.* 36, 1657–1668.
- Bao, Q., Lou, Y., Xing, T., et al., 2013. Rapid synthesis of zeolitic imidazolate framework-8 (ZIF-8) in aqueous solution via microwave irradiation. *Inorg. Chem. Commun.* 37, 170–173.
- Batool, M., Abbas, M.A., Khan, I.A., et al., 2023. Response surface methodology modeling correlation of polymer composite carbon nanotubes/chitosan nanofiltration membranes for water desalination. *ACS ES&T Water.* 3, 1406–1421.
- Bian, S., Wang, Y., Xiao, F., et al., 2022. Fabrication of polyamide thin-film nanocomposite reverse osmosis membrane with improved permeability and antibacterial performances using silver immobilized hollow polymer nanospheres. *Desalinization* 539, 115953.
- Cao, S.-L., Xu, H., Lai, L.-H., et al., 2017. Magnetic ZIF-8/cellulose/Fe₃O₄ nanocomposite: Preparation, characterization, and enzyme immobilization. *Bioresour. Bioprocess.* 4, 1–7.
- Childress, A.E., Elimelech, M., 2000. Relating nanofiltration membrane performance to membrane charge (electrokinetic) characteristics. *Environ. Sci. Tech.* 34, 3710–3716.
- Choi, S.-W., Kim, T.-H., Jo, S.-W., et al., 2018. Hydrocarbon membranes with high selectivity and enhanced stability for vanadium redox flow battery applications: Comparative study with sulfonated poly (ether sulfone) s and sulfonated poly (thioether ether sulfone) s. *Electrochim. Acta* 259, 427–439.
- Cigeroglu, Z., El Messaoudi, N., Şenol, Z.M., et al., 2024. Clay-based nanomaterials and their adsorptive removal efficiency for dyes and antibiotics: a review. *Mater. Today Sustain.* 100735.
- Cohen-Tanugi, D., Grossman, J.C., 2012. Water desalination across nanoporous graphene. *Nano Lett.* 12, 3602–3608.
- Costa, B.A., Abuqafy, M.P., Barbosa, T.W.L., et al., 2023. ZnO@ ZIF-8 nanoparticles as nanocarrier of ciprofloxacin for antimicrobial activity. *Pharmaceutics* 15, 259.
- Daneshvar, N., Aleboye, A., Khataee, A., 2005. The evaluation of electrical energy per order (EEO) for photooxidative decolorization of four textile dye solutions by the kinetic model. *Chemosphere* 59, 761–767.
- Daraei, P., Madaeni, S.S., Ghaemi, N., et al., 2013. Fabrication of PES nanofiltration membrane by simultaneous use of multi-walled carbon nanotube and surface graft polymerization method: comparison of MWCNT and PAA modified MWCNT. *Sep. Purif. Technol.* 104, 32–44.
- Du, S., Zhao, P., Wang, L., et al., 2023. Progresses of advanced anti-fouling membrane and membrane processes for high salinity wastewater treatment. *Results Eng.* 100995.
- Dutta, S., Gupta, B., Srivastava, S.K., et al., 2021. Recent advances on the removal of dyes from wastewater using various adsorbents: A critical review. *Mater. Adv.* 2, 4497–4531.
- Ebrahimi, M., Van der Bruggen, B., Hosseini, S., et al., 2019. Improving electrochemical properties of cation exchange membranes by using activated carbon-co-chitosan composite nanoparticles in water deionization. *Ionics* 25, 1199–1214.
- Edo, G.I., Itoje-akpokiniyo, L.O., Obasohan, P., et al., 2024. Impact of environmental pollution from human activities on water, air quality and climate change. *Ecol. Front.*
- El-habacha, M., Miyah, Y., Lagdali, S., et al., 2023. General overview to understand the adsorption mechanism of textile dyes and heavy metals on the surface of different clay materials. *Arab. J. Chem.* 16, 105248.
- Eskikaya, O., Kucukosman, R., Ozdemir, S., et al., 2024. Investigation of the treatment and antibacterial properties of pollutant-containing water using black phosphorus blended polyethersulfone membranes (BP@ PES). *J. Water Process Eng.* 57, 104581.
- Fan, X., Wei, G., Quan, X., 2023. Carbon nanomaterial-based membranes for water and wastewater treatment under electrochemical assistance. *Environ. Sci. Nano* 10, 11–40.
- Farahani, S.K., Hosseini, S.M., 2022. A highly promoted nanofiltration membrane by incorporating of aminated Zr-based MOF for efficient salts and dyes removal with excellent antifouling properties. *Chem. Eng. Res. Des.* 188, 764–778.
- Farjami, M., Moghadassi, A., Vatanpour, V., et al., 2019. Preparation and characterization of a novel high-flux emulsion polyvinyl chloride (EPVC) ultrafiltration membrane incorporated with boehmite nanoparticles. *J. Ind. Eng. Chem.* 72, 144–156.
- Farjami, M., Moghadassi, A., Vatanpour, V., 2021. Influence of solvent type on the ability and properties of the boehmite nanoparticles embedded emulsion polyvinyl chloride nanocomposite ultrafiltration membranes. *Iran. Polym. J.* 30, 707–721.
- Fu, M., Wang, C., Sun, G., et al., 2022. Controllable preparation of acid and alkali resistant 3D flower-like UiO-66-NH₂/ZIF-8 imbedding PPTA composite nanofiltration membrane for dye wastewater separation. *J. Water Process Eng.* 50, 103320.
- Furukawa, H., Cordova, K.E., O'Keeffe, M., et al., 2013. The chemistry and applications of metal-organic frameworks. *Science* 341, 1230444.
- Ganji, P., Nazari, S., Zinatizadeh, A., et al., 2022. Chitosan-wrapped multi-walled carbon nanotubes (CS/MWCNT) as nanofillers incorporated into nanofiltration (NF) membranes aiming at remarkable water purification. *J. Water Process Eng.* 48, 102922.
- Gao, Q., Bouwen, D., Yuan, S., et al., 2023. Robust loose nanofiltration membrane with fast solute transfer for dye/salt separation. *J. Membr. Sci.* 674, 121518.
- Gao, Y., Wang, K., Wang, X.-M., et al., 2022. Exploitation of amine groups cooped up in polyamide nanofiltration membranes to achieve high rejection of micropollutants and high permeance of divalent cations. *Environ. Sci. Tech.* 56, 10954–10962.

- George, J., Kumar, V.V., 2023. Polymeric membranes customized with super paramagnetic iron oxide nanoparticles for effective separation of pentachlorophenol and proteins in aqueous solution. *J. Mol. Struct.* 1284, 135449.
- Ghiggi, F.F., Pollo, L.D., Cardozo, N.S., et al., 2017. Preparation and characterization of polyethersulfone/N-phthaloyl-chitosan ultrafiltration membrane with antifouling property. *Eur. Polym. J.* 92, 61–70.
- Giri, T.K., Badwaik, H., 2022. Understanding the application of gum ghatti based biodegradable hydrogel for wastewater treatment. *Environ. Nanotechnol. Monit. Manage.* 17, 100668.
- Goh, P., Ismail, A., 2018. A review on inorganic membranes for desalination and wastewater treatment. *Desalination* 434, 60–80.
- Goh, K., Karahan, H.E., Wei, L., et al., 2016. Carbon nanomaterials for advancing separation membranes: A strategic perspective. *Carbon* 109, 694–710.
- Gowriboy, N., Kalaivizhi, R., Ganesh, M., et al., 2022a. Development of thin film polymer nanocomposite membrane (ZIF-8@ PSF/CS) for removal of textile pollutant and evaluating the effect of water samples on human monocytic cell lines (THP-1) using flow cytometer. *J. Clean. Prod.* 377, 134399.
- Gowriboy, N., Kalaivizhi, R., Kaleekkal, N.J., et al., 2022b. Fabrication and characterization of polymer nanocomposites membrane (Cu-MOF@ CA/PES) for water treatment. *J. Environ. Chem. Eng.* 10, 108668.
- Halek, F.S., Farahani, S.K., Hosseini, S.M., 2016. Fabrication of poly (ether sulfone) based mixed matrix membranes modified by TiO₂ nanoparticles for purification of biodiesel produced from waste cooking oils. *Korean J. Chem. Eng.* 33, 629–637.
- He, X., Liu, X., Liu, J., et al., 2024. Self-assembled superhydrophilic MOF-decorated membrane for highly efficient treatment and separation mechanism of multi-component emulsions. *Desalination* 569, 117047.
- Hema, M., Arivoli, S., 2007. Comparative study on the adsorption kinetics and thermodynamics of dyes onto acid activated low cost carbon. *Int. J. Phys. Sci.* 2, 10–17.
- Hosseini, S., Amini, S., Khodabakhshi, A., et al., 2018. Activated carbon nanoparticles entrapped mixed matrix polyethersulfone based nanofiltration membrane for sulfate and copper removal from water. *J. Taiwan Inst. Chem. Eng.* 82, 169–178.
- Hosseini, S., Afshari, M., Fazlali, A., et al., 2019. Mixed matrix PES-based nanofiltration membrane decorated by (Fe₃O₄-polyvinylpyrrolidone) composite nanoparticles with intensified antifouling and separation characteristics. *Chem. Eng. Res. Des.* 147, 390–398.
- Hosseini, S.M., Karami, F., Farahani, S.K., et al., 2020. Tailoring the separation performance and antifouling property of polyethersulfone based NF membrane by incorporating hydrophilic CuO nanoparticles. *Korean J. Chem. Eng.* 37, 866–874.
- Hosseini, S.M., Moradi, F., Farahani, S.K., et al., 2021. Carbon nanofibers/chitosan nanocomposite thin film for surface modification of poly (ether sulphone) nanofiltration membrane. *Mater. Chem. Phys.* 269, 124720.
- Hosseini, S.M., Mohammadianfar, S., Farahani, S.K., et al., 2023. Polyether sulfone-graphite nanocomposite for nanofiltration membrane with enhanced separation, antifouling and antibacterial properties. *Korean J. Chem. Eng.* 40, 185–194.
- Jacob, J., Peter, G., Thomas, S., et al., 2019. Chitosan and polyvinyl alcohol nanocomposites with cellulose nanofibers from ginger rhizomes and its antimicrobial activities. *Int. J. Biol. Macromol.* 129, 370–376.
- Kali, R., Mkandawire, W.D., Milner, S.T., 2023. Optimizing the structure and performance of biomimetic water channels. *Mol. Syst. Des. Eng.* 8, 443–450.
- Kamari, S., Shahbazi, A., 2021. High-performance nanofiltration membrane blended by Fe₃O₄@ SiO₂-CS bionanocomposite for efficient simultaneous rejection of salts/heavy metals ions/dyes with high permeability, retention increase and fouling decline. *Chem. Eng. J.* 417, 127930.
- Karami, S., Jiriaei Sharahi, Z., Koudzari Farahani, S., et al., 2023. Novel thin-film, chitosan-polyaniline nanofiltration membrane effectively removes toxic heavy metals from wastewaters. *Iran. J. Toxicol.* 17.
- Karan, S., Jiang, Z., Livingston, A.G., 2015. Sub-10 nm polyamide nanofilms with ultrafast solvent transport for molecular separation. *Science* 348, 1347–1351.
- Keshvardostchokami, M., Majidi, M., Zamani, A., et al., 2021. Adsorption of phenol on environmentally friendly Fe₃O₄/chitosan/zeolitic imidazolate framework-8 nanocomposite: Optimization by experimental design methodology. *J. Mol. Liq.* 323, 115064.
- Khajavian, M., Salehi, E., Vatanpour, V., 2020a. Chitosan/polyvinyl alcohol thin membrane adsorbents modified with zeolitic imidazolate framework (ZIF-8) nanostructures: Batch adsorption and optimization. *Sep. Purif. Technol.* 241, 116759.
- Khajavian, M., Salehi, E., Vatanpour, V., 2020b. Nanofiltration of dye solution using chitosan/poly (vinyl alcohol)/ZIF-8 thin film composite adsorptive membranes with PVDF membrane beneath as support. *Carbohydr. Polym.* 247, 116693.
- Khajavian, M., Shahsavari, S., Salehi, E., et al., 2021. Ethylenediamine-functionalized ZIF-8 for modification of chitosan-based membrane adsorbents: batch adsorption and molecular dynamic simulation. *Chem. Eng. Res. Des.* 175, 131–145.
- Khan, I.A., Ahmad, N.M., 2023. Activated carbon, CNTs and GO based polymeric nanocomposites membranes for textile wastewater treatment: preparation, performance, and fouling control. *Environ. Sci. Proc.* 25, 77.
- Kharraz, J.A., An, A.K., 2020. Patterned superhydrophobic polyvinylidene fluoride (PVDF) membranes for membrane distillation: Enhanced flux with improved fouling and wetting resistance. *J. Membr. Sci.* 595, 117596.
- Khoerunnisa, F., Amanda, P.C., Nurhayati, M., et al., 2023. Promotional effect of ammonium chloride functionalization on the performance of polyethersulfone/chitosan composite-based ultrafiltration membrane. *Chem. Eng. Res. Des.* 190, 366–378.
- Khosravi, M.J., Hosseini, S.M., Vatanpour, V., 2022. Polyamidoamine dendrimers-Mil-125 (Ti) MOF embedded polyethersulfone membrane for enhanced removal of heavy metal, antibiotic and dye from water. *J. Environ. Chem. Eng.* 10, 108644.
- Langbehn, R.K., Michels, C., Soares, H.M., 2021. Antibiotics in wastewater: From its occurrence to the biological removal by environmentally conscious technologies. *Environ. Pollut.* 275, 116603.
- Li, Y., Li, J., Zhu, D., et al., 2023. Facile dual-functionalization of NF membranes with excellent chlorine resistance and good antifouling property by in-situ grafting of zwitterions. *Sep. Purif. Technol.* 315, 123660.
- Liu, X., Wang, J., 2024. Decolorization and degradation of various dyes and dye-containing wastewater treatment by electron beam radiation technology: an overview. *Chemosphere* 141255.
- Low, Z.-X., Ji, J., Blumenstock, D., et al., 2018. Fouling resistant 2D boron nitride nanosheet-PES nanofiltration membranes. *J. Membr. Sci.* 563, 949–956.
- Makhetha, T., Moutloali, R., 2018. Antifouling properties of Cu (tpa)@ GO/PES composite membranes and selective dye rejection. *J. Membr. Sci.* 554, 195–210.
- Makhetha, T., Moutloali, R., 2021. Incorporation of a novel Ag-Cu@ ZIF-8@ GO nanocomposite into polyethersulfone membrane for fouling and bacterial resistance. *J. Membr. Sci.* 618, 118733.
- Miao, J., Chen, G., Gao, C., et al., 2008. Preparation and characterization of N, O-carboxymethyl chitosan/Polysulfone composite nanofiltration membrane crosslinked with epichlorohydrin. *Desalination* 233, 147–156.
- Mirzamoammadi, M., Koudzari Farahani, S., Parvizian, F., et al., 2021. Surface Modification of Nanofiltration Membrane Using Poly (vinyl alcohol) and Chitosan-Functionalized Activated Carbon Nanoparticles. *Iran. J. Polym. Sci. Technol. (persian)* 34, 349–358.
- Moghaddasi, A., Ghohyeh, S., Bandehali, S., et al., 2023. Cuprous oxide (Cu₂O) nanoparticles in nanofiltration membrane with enhanced separation performance and anti-fouling properties. *Korean J. Chem. Eng.* 40, 630–641.
- Mohammadifakhr, M., Trzaskus, K., Kemperman, A., et al., 2020. Increasing the success rate of interfacial polymerization on hollow fibers by the single-step addition of an intermediate layer. *Desalination* 491, 114581.
- Moradi, G., Heydari, R., Zinadini, S., et al., 2021. High-performance nanofiltration membranes consisting of the new functionalized mesoporous for enhanced antifouling attributes and simultaneous removal of salts, dyes and heavy metals. *Environ. Technol. Innov.* 24, 101929.
- Moradi, G., Heydari, R., Zinadini, S., et al., 2022. Fouling alleviation and enhanced salt rejection in NF membranes via incorporation of 5-amino-1-phenyl-3-(thiophen-2-yl)-1H-pyrazole-4-carbonitrile functionalized pectin in PES matrix. *J. Water Process Eng.* 48, 102888.
- Moradi, G., Heydari, R., Zinadini, S., et al., 2023a. Chitosan-furoseme/pectin surface functionalized thin film nanofiltration membrane with improved antifouling behavior for pharmaceutical wastewater treatment. *J. Ind. Eng. Chem.* 124, 368–380.
- Moradi, G., Zinadini, S., Rahimi, M., 2023b. The enhancement in dye removal and antifouling capability of PES nanofiltration membrane modified with fumarate-alumoxane nanoparticles. *J. Appl. Res. Water Wastewater.* 10, 161–166.
- Morgante, C., Lopez, J., Cortina, J., et al., 2024. New generation of commercial nanofiltration membranes for seawater/brine mining: Experimental evaluation and modelling of membrane selectivity for major and trace elements. *Sep. Purif. Technol.* 340, 126758.
- Naik, N.S., Padaki, M., Isloor, A.M., et al., 2021. Poly (ionic liquid)-Based charge and size selective loose nanofiltration membrane for molecular separation. *Chem. Eng. J.* 418, 129372.
- Nasrollahi, N., Aber, S., Vatanpour, V., et al., 2019. Development of hydrophilic microporous PES ultrafiltration membrane containing CuO nanoparticles with improved antifouling and separation performance. *Mater. Chem. Phys.* 222, 338–350.
- Natrayan, L., P. Arul Kumar, J. A. Dhanraj, et al., 2022. Synthesis and analysis of impregnation on activated carbon in multiwalled carbon nanotube for Cu adsorption from wastewater. *Bioinorg. Chem. Appl.* 2022.
- Nellur, U., Naik, N.S., Rego, R.M., et al., 2023. Ce-MOF infused membranes with enhanced molecular sieving in the application of dye rejection. *Environ. Sci. Water Res. Technol.* 9, 1216–1230.
- Oulad, F., Zinadini, S., Zinatizadeh, A.A., et al., 2024. Development and investigation of high-flux antifouling NF PES membranes decorated by aniline oligomers and application for wastewater treatment. *Polym. Adv. Technol.* 35, e6234.
- Rezania, J., Shockravi, A., Vatanpour, V., et al., 2019. Preparation and performance evaluation of carboxylic acid containing polyamide incorporated microporous ultrafiltration PES membranes. *Polym. Adv. Technol.* 30, 407–416.
- Safarpour, M., Vatanpour, V., Khataee, A., 2016. Preparation and characterization of graphene oxide/TiO₂ blended PES nanofiltration membrane with improved antifouling and separation performance. *Desalination* 393, 65–78.
- Sahu, A., Dosi, R., Kwiatkowski, C., et al., 2023. Advanced polymeric nanocomposite membranes for water and wastewater treatment: a comprehensive review. *Polymers* 15, 540.
- Salehi, E., Khajavian, M., Sahebamee, N., et al., 2022. Advances in nanocomposite and nanostructured chitosan membrane adsorbents for environmental remediation: A review. *Desalination* 527, 115565.
- Samari, M., Heydari, R., Gholami, F., 2024. Nanofiltration membrane functionalized with Cu₂P nanoparticles: A promising approach for enhanced pesticide removal and long-term stability. *J. Clean. Prod.* 445, 141352.
- Seidypoor, A., Bandehali, S., Ebrahimi, M., et al., 2023. Fabrication of layer-by-layer ion exchange membrane by applying PDA-POSS nanocomposite onto heterogeneous cationic substrate for water treatment. *Colloid Nanosci. J.* 1, 51–61.
- Shahid, M.U., Najam, T., Islam, M., et al., 2024. Engineering of metal organic framework (MOF) membrane for waste water treatment: Synthesis, applications and future challenges. *J. Water Process Eng.* 57, 104676.

- Shao, X., Yao, G., Wang, Z., et al., 2024. MOFs and surface modification synergistically modulated cellulose membranes for enhanced water permeability and efficient tellurium separation in wastewater. *J. Clean. Prod.* 434, 139873.
- Sharma, M., Alves, P., Gando-Ferreira, L.M., 2023a. Effect of activated carbon nanoparticles on the performance of PES nanofiltration membranes to separate kraft lignin from black liquor. *J. Water Process Eng.* 52, 103487.
- Sharma, U., Pandey, R., Basu, S., et al., 2023b. ZIF-67 blended PVDF membrane for improved Congo red removal and antifouling properties: A correlation establishment between morphological features and ultra-filtration parameters. *Chemosphere* 320, 138075.
- Shukla, S., Khan, R., Daverey, A., 2021. Synthesis and characterization of magnetic nanoparticles, and their applications in wastewater treatment: A review. *Environ. Technol. Innov.* 24, 101924.
- Sinha Ray, S., Singh Bakshi, H., Dangayach, R., et al., 2020. Recent developments in nanomaterials-modified membranes for improved membrane distillation performance. *Membranes* 10, 140.
- Sun, Q., Song, Z., Liu, H., et al., 2023. Smart pH-responsive covalent organic framework membrane for charge-driven molecular sieving. *Chem. Mater.* 35, 7847–7858.
- Szczęśniak, B., Choma, J., Jaroniec, M., 2018. Tailoring surface and structural properties of composite materials by coupling Pt-decorated graphene oxide and ZIF-8-derived carbon. *Appl. Surf. Sci.* 459, 760–766.
- Ullah, A., Tanudjaja, H.J., Ouda, M., et al., 2021. Membrane fouling mitigation techniques for oily wastewater: A short review. *J. Water Process Eng.* 43, 102293.
- Varma, V.C., Rathinam, R., Suresh, V., et al., 2024. Urban waste water management paradigm evolution: Decentralization, resource recovery, and water reclamation and reuse. *Environ. Qual. Manag.* 33, 523–540.
- Vatanpour, V., Naeeni, R.S.E., Ghadimi, A., et al., 2018. Effect of detonation nanodiamond on the properties and performance of polyethersulfone nanocomposite membrane. *Diam. Relat. Mater.* 90, 244–255.
- Vatanpour, V., Karimi, H., Ghazanlou, S.I., et al., 2020. Anti-fouling polyethersulfone nanofiltration membranes aided by amine-functionalized boron nitride nanosheets with improved separation performance. *J. Environ. Chem. Eng.* 8, 104454.
- Vatanpour, V., Ardic, R., Esenli, B., et al., 2024. Defected Ag/Cu-MOF as a modifier of polyethersulfone membranes for enhancing permeability, antifouling properties and heavy metal and dye pollutant removal. *Sep. Purif. Technol.* 345, 127336.
- Wang, T.-X., Chen, S.-R., Wang, T., et al., 2022. PES mixed-matrix ultrafiltration membranes incorporating ZIF-8 and poly (ionic liquid) by microemulsion synthetic with flux and antifouling properties. *Appl. Surf. Sci.* 576, 151815.
- Wang, J., Li, Y., Lv, Z., et al., 2019. Exploration of the adsorption performance and mechanism of zeolitic imidazolate framework-8@ graphene oxide for Pb (II) and 1-naphthylamine from aqueous solution. *J. Colloid Interface Sci.* 542, 410–420.
- Wang, C., Wang, H., Luo, R., et al., 2017. Metal-organic framework one-dimensional fibers as efficient catalysts for activating peroxymonosulfate. *Chem. Eng. J.* 330, 262–271.
- Wang, Z., Zhang, W., Wen, S., et al., 2023. Rapid co-deposition of dopamine and polyethyleneimine triggered by CuSO₄/H₂O₂ oxidation to fabricate nanofiltration membranes with high selectivity and antifouling ability. *Sep. Purif. Technol.* 305, 122409.
- Wu, C., Dai, X., Sun, X., et al., 2023. Preparation and characterization of fluoroalkyl activated carbons/PVDF composite membranes for water and resources recovery by membrane distillation. *Sep. Purif. Technol.* 305, 122519.
- Xiong, Y., Deng, N., Wu, X., et al., 2022. De novo synthesis of amino-functionalized ZIF-8 nanoparticles: Enhanced interfacial compatibility and pervaporation performance in mixed matrix membranes applying for ethanol dehydration. *Sep. Purif. Technol.* 285, 120321.
- Yao, Y.-Y., Wang, T., Wu, L.-G., et al., 2022. PES mixed-matrix membranes incorporating ZIF-8@ MXene nanocomposite for the efficient dye/salt separation. *Desalination* 543, 116116.
- Yu, Q., Zhou, Y., Gao, C., 2024. UiO-66 regulated thin-film nanocomposite membranes for water treatment. *Desalination* 117917.
- Zareei, F., Bandehali, S., Parvizian, F., et al., 2021. Promoting the separation and antifouling properties of polyethersulfone-based nanofiltration membrane by incorporating of cobalt ferrite/activated carbon composite nanoparticles. *Chem. Eng. Res. Des.* 169, 204–213.
- Zareei, F., Hosseini, S.M., 2019. A new type of polyethersulfone based composite nanofiltration membrane decorated by cobalt ferrite-copper oxide nanoparticles with enhanced performance and antifouling property. *Sep. Purif. Technol.* 226, 48–58.
- Zhang, R., Li, Y., Yan, J., Zeng, J., et al., 2023. Surface modification of pvdf membranes with quaternized chitosan for selective separation of negatively charged polysaccharides—exemplified with Heparin. *J. Environ. Chem. Eng.* Available at SSRN 4372912.
- Zhang, Z., Yan, Y., Chen, Y., et al., 2014. Investigation of CO₂ absorption in methyldiethanolamine and 2-(1-piperazinyl)-ethylamine using hollow fiber membrane contactors: Part C. Effect of operating variables. *J. Nat. Gas Sci. Eng.* 20, 58–66.
- Zhao, J., Cao, L., Wang, X., et al., 2023. MOF@ Polydopamine-incorporated membrane with high permeability and mechanical property for efficient fouling-resistant and oil/water separation. *Environ. Res.* 116685.
- Zheng, H., Zhu, M., Wang, D., et al., 2023. Surface modification of PVDF membrane by CNC/Cu-MOF-74 for enhancing antifouling property. *Sep. Purif. Technol.* 306, 122599.
- Zinadini, S., Rostami, S., Vatanpour, V., et al., 2017. Preparation of antibiofouling polyethersulfone mixed matrix NF membrane using photocatalytic activity of ZnO/MWCNTs nanocomposite. *J. Membr. Sci.* 529, 133–141.